1-1-2009

A new CEM_{43} thermal dose model based on Vogel-Tammann-Fulcher behaviour in thermal damage processes

Hisham Assi
Ryerson University

A NEW CEM_{43} THERMAL DOSE MODEL BASED ON VOGEL–TAMMANN–FULCHER BEHAVIOUR IN THERMAL DAMAGE PROCESSES

by

Hisham Assi

B.Sc, Birzeit University, Palestine, 1997

A thesis

presented to Ryerson University

in partial fulfillment of the

requirement for the degree of

Master of Science

in the Program of

Biomedical Physics.

Toronto, Ontario, Canada, 2009

Author's Declaration

I hereby declare that I am the sole author of this thesis.

I authorize Ryerson University to lend this thesis to other institutions or individuals for the purpose of scholarly research.

HISHAM ASSI

I further authorize Ryerson University to reproduce this thesis by photocopying or by other means, in total or in part, at the request of other institutions or individuals for the purpose of scholarly research.

HISHAM ASSI

Instructions on Borrowers

Ryerson University requires the signatures of all persons using or photocopying this thesis. Please sign below, and give address and date.

Abstract

Hisham Assi, "A New CEM_{43} Thermal Dose Model Based on Vogel–Tammann–Fulcher Behaviour in Thermal Damage Processes", MSc, Biomedical Physics, Ryerson University, Toronto, 2009

Thermal dose models are metrics that quantify thermal damage in tissues based on the temperature and the time of exposure. The validity and accuracy of one of the commonly used models (CEM_{43}) for high temperature thermal therapy applications (50–90°C) is questionable. It was found to over-estimate the accumulation of thermal damage for high-temperature applications. A new CEM_{43} dose model based on Arrhenius type Vogel-Tammann-Fulcher equation using published data is introduced in this work. The new dose values for the same damage threshold that was produced at different *in-vivo* skin experiments were in the same order of magnitude, while the current dose values were 2 orders of magnitude different. The new dose values for same damage threshold in 6 lesions in *ex-vivo* liver experiments were more consistent than the current dose values. Computer simulations of laser interstitial thermal therapy showed that the current model usually predicts bigger volume than the new model does. The deviation in damaged volume prediction can be significant. The contribution of this work is introducing methods that can lead to more robust thermal dosimetry which will result in improved thermal therapy modelling, monitoring, and control.

Acknowledgments

I would like to thank my supervisors Dr. Carl Kumaradas and Dr. William Whelan for their guidance and support throughout my master study. Thank you for encouraging me to investigate and for teaching me how to become a researcher. I am very grateful that you gave me the opportunity to be one of your students.

Additionally, I would like thank my supervisory committee members for advising me on my project and for their critical questions: Dr. Catherine Beauchemin and Dr. Lee Chin.

Furthermore, I would like to thank Michel Arsenault from Dr. Whelan's lab at UPEI for the detailed data of his experiments.

Finally, I would like to thank my colleagues and all physics department members for the supportive friendly environment.

This thesis is dedicated to Falastine.

Contents

List of Figures

Nomenclature

A	Frequency factor [s^{-1}]
a	Parameter related to activation energy [K]
c_b	Specific heat of blood [J kg^{-1} K^{-1}]
c_t	Specific heat of tissue [J kg^{-1} K^{-1}]
D_c	Diffusion coefficient [m]
E_a	Activation energy [J $mole^{-1}$]
k	Reaction velocity or rate constant [s^{-1}]
k_t	Thermal conductivity of tissue [W m^{-1} K^{-1}]
L	Length of the diffusing tip [m]
μ_a	Optical absorption coefficient [m^{-1}]
$\mu_s^{'}$	Optical reduced scattering coefficient [m^{-1}]
$\mu_{s\_denatured}^{'}$	Reduced scattering coefficient of denatured tissue [m^{-1}]
$\mu_{s\_native}^{'}$	Reduced scattering coefficient of native tissue [m^{-1}]
P	Laser power [W]
Q	Heat source [W m^{-3}]
ρ_t	Density of tissue [kg m^{-3}]
R	The universal gas constant [8.23 J $mole^{-1}K^{-1}$]
$\mathbf{r}$	Position vector [m]
r_0	Fibre radius [m]
S	Absorbed power density [W m^{-3}]
τ	Total heating time [s]
T	Arbitrary constant temperature [°C]
T_0	System-based absolute temperature [°C]

t_{43}	Dose value using the current CEM_{43} model [eq.min]
t'_{43}	Dose value using the new CEM_{43} model [eq.min]
$t_{43\_critical}$	Thermal dose threshold for onset of damage [eq.min]
T_b	Blood temperature [37°C]
$T(t)$	Time-varying temperature [°C]
ϕ	Optical fluence rate [W m^{-2}]
Ω	Dose value using Arrhenius–like models [Dimensionless]
ω_b	Blood perfusion [kg m^{-3} s^{-1}]
ω_{b0}	Baseline blood perfusion [kg m^{-3} s^{-1}]

Abbreviations

CT	Computed Tomography
CEM_{43}	Cumulative Equivalent Minutes at 43°C
HIFU	High Intensity Focused Ultrasound
LITT	Laser Interstitial Thermal Therapy
MRI	Magnetic Resonance Imaging
VTF	Vogel-Tammann-Fulcher

Chapter 1

Introduction

1.1 Thermal Therapy

Quantifying the amount of thermal damage in biological systems based on thermal exposure (time and temperature of exposure) has been an active area of research for more than 60 years[2,3,5,6]. Earlier, these studies focused mainly on skin burns[2,3,7]. The importance of heat-induced tissue damage studies has grown since heat started being used as a cancer treatment. Thermal therapy, which is a cancer treatment, can be divided into two types. In hyperthermia tissues are exposed to temperatures of 42°C to 46°C to kill cancer cells or to make them more sensitive to radiation therapy[8] or other treatment modalities. Coagulative thermal therapy, where higher temperatures (50°C to 90°C) are used, is a stand-alone thermal therapy which targets small localized solid tumours to destroy them by coagulation[9–14]. Many sources of energy, including laser[9,10], microwave[11], and ultrasound[12–14] are being investigated for tissue heating. Each of them has its advantages and disadvantages. Some thermal therapies are non-invasive, like high intensity focused ultrasound (HIFU) while others are minimally invasive such as laser interstitial thermal therapy (LITT). In LITT, laser energy is directly delivered to the tumour through one or more optical fibres inserted into the tissue. LITT is presented in detail in section 2.3 as a clinical application of thermal dose

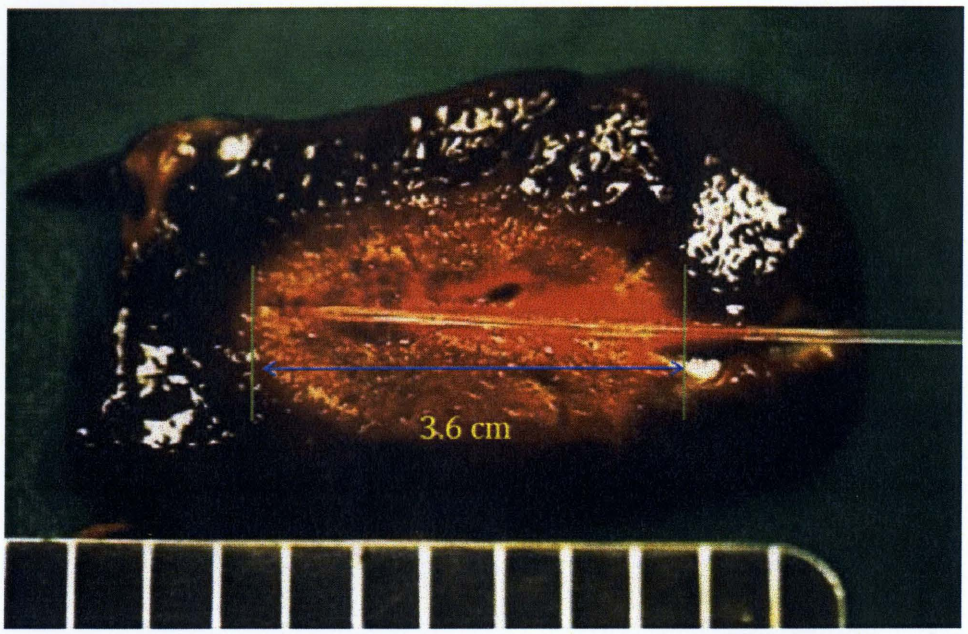

Figure 1.1: LITT experiment in *ex-vivo* porcine liver adapted from Heisterkamp *et al*[1]. The lesion was created using 6 W laser for 6 minutes. Lesion with this size can not be created *in vivo* because the cooling effect of blood perfusion.

methods.

1.2 Thermal Therapy Monitoring Techniques

The main challenge in thermal therapy is to destroy the tumour while sparing the surrounding healthy tissue and vital organs. Unlike the LITT *ex-vivo* experiment shown in figure 1.1 where the damage extent can be easily observed, knowing the damage extent and the damage boundary location for *in-vivo* treatments is a difficult task. Hence, monitoring techniques are needed. Monitoring techniques that are being used and investigated include image-based monitoring using magnetic resonance imaging[11,12,15,16], computed tomography[1,17], and ultrasound imaging[18], and point-based monitoring using temperature[9,19,20] and light based[21] point measurements. Real-time monitoring of the coagulation progression during treatment is vital in thermal therapy. It provides critical information to keep heating until the entire tumour is damaged, or to stop to prevent vital organ's damage.

Image-based monitoring

Ultrasonography: Ultrasound imaging is usually used to guide accurate placement of catheters into tumours. Real-time monitoring of thermal therapy using ultrasound has been investigated[18], but the echogenic area that is observed during the treatment is believed to be caused by gas bubbles which does not represent the damaged area[1]. Ultrasound imaging is also problematic in evaluating damage after treatment since the echogenic area sometimes becomes heterogeneous in minutes[1].

Computed tomography: CT can be used for the diagnostic assessment before treatment. Within 4 days after the treatment, contrast-enhanced CT shows the non-perfused treated region very clearly as a well defined non-enhanced area in contrast with the untreated perfused area[1]. Real-time monitoring using CT has been investigated using dynamic contrast enhanced CT[17], but data collection takes a long time making real time monitoring using CT impractical.

Magnetic resonance imaging: MRI can be used for diagnostics, guidance for catheter placement and for evaluating damage extent after the treatment. In addition, MRI can be used in real-time monitoring of thermal therapy during treatment. *Directly* monitoring the progression of thermal damage by detecting structural changes during the treatment may underestimate thermal damage extent[11,15]. This may be due to the delay in damage manifestation in locations where exposure is less than that needed to cause immediate structural changes[11]. Therefore temperature maps produced during the treatment using MRI, can be used to predict damage. Some studies use the temperature, *directly*, as a threshold to defined damage[16]. Since temperature alone, regardless of exposure time, does not necessarily correlate with damage, time-temperature history should be used in quantifying thermal damage. This has been done in many studies[11,12,14] which showed a good match with histology and other after-treatment results.

Point-based monitoring

MRI is useful for real-time monitoring, but depending on it alone will limit the adoption of thermal therapy due to the cost, the size, and availability problems of MRI machines. Other real-time monitoring techniques, like point-monitoring, have been investigated for inexpensive real-time monitoring.

Temperature-based point monitoring is being used in real time monitoring of thermal therapy.[9,19,20] Sensors are placed in critical locations like tumour boundary, close to vital organs, or at close to the power source to record temperatures during the treatment. The temperature history information at these points can guide decisions on whether to stop the treatment. It also can be used for dynamic feedback in thermal therapy control systems.

Optical-based point monitoring is also being investigated. Taking advantage of the significant changes in tissue optical scattering properties due to coagulation, temporal profile of light intensity at a single point can be used to obtain global information about the progression of thermal damage[21].

Many of the monitoring techniques give information about temperature history at a given location. What is more relevant is the amount of thermal damage at that location. Hence, a *reliable* method to quantify the *end point* of thermal damage, based on the time-temperature information, is needed. These methods depends on thermal dose models.

1.3 Thermal Dose

Thermal dose is not simply a measure of the amount of energy delivered. Rather, it is a measure of the amount of tissue damage caused by heat. An ideal thermal dose model should predict the same dose for the same damage (i.e. biological endpoint) regardless of the heating protocol used (i.e. the time-temperature combination). Thermal damage, or heat-induced cell death, is believed to be caused by protein denaturation, for the range of temperatures used in thermal therapy[22–24]. The first thermal dose model, known as the

Arrhenius model (equation 2.2), was introduced by Henriques in 1947[3] based on rate process analysis. In this model, thermal damage is quantified by a single parameter (denoted by Ω) which depends on the time-temperature profile and two tissue-dependent parameters that are experimentally determined for each type of tissue. Henriques found the parameters based on *in vivo* experiments for both porcine and human skin[2]. In those experiments, time-temperature combinations to achieve the same thermal damage end point (7 days later) were obtained. Damage can continue to occur after the completion of the treatment. The fact that dose models have been developed using the final damage as an end-point is very important, because this will lead to predicting the final damage when these models are used. The Arrhenius parameters reported for certain tissue type in different studies are significantly different[25], which raises a problem with using the Arrhenius dose model. This thesis provides an alternative modified Arrhenius equation for thermal damage analysis which might solve this problem.

Another commonly used thermal dose model is the CEM_{43} model (equation 2.4) which was originally introduced by Sapareto and Dewey in 1984[5]. This is an empirical model that quantifies damage by the exposure time at some reference temperature. 43°C was arbitrary chosen as the reference, where all thermal exposures are converted to "equivalent minutes" [eq.min] at this temperature. The time-temperature relationship on which this conversion is based was suggested by many experimental observations of different biological systems[2,8,26]. In most biological systems, a 1°C *increase* in temperature requires half the time for the same effect above 43°C and one-fourth of the time below 43°C. For example, if a certain thermal damage threshold can be achieved by heating at constant temperature of 43°C for 200 minutes, the CEM_{43} model would predict that the same threshold could be also achieved by heating at other time-temperature combinations such as those shown in figure 1.2 where the dose for each combination is: $t_{43} = 200$ [eq.min].

This relationship does not assume, nor does it require, that different tissues have the same thermal sensitivity. Hence, the CEM_{43} model can be used for different tissue types

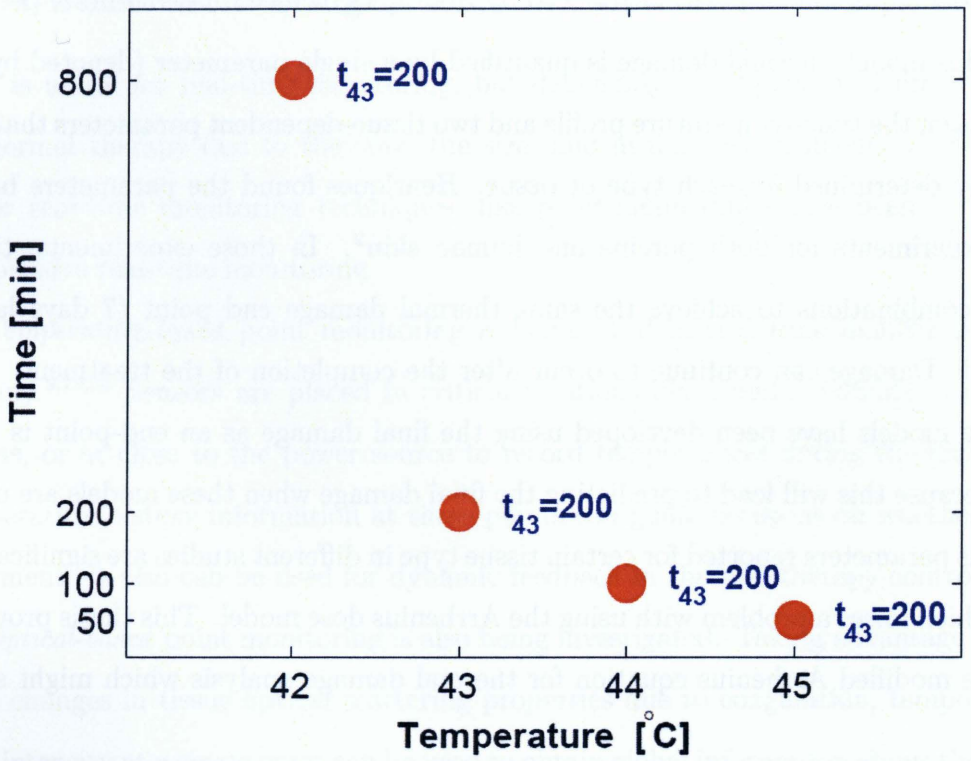

Figure 1.2: Four time-temperature combinations which would result in the same damage threshold (200 eq.min) according to the Sapareto and Dewey,CEM_{43}, dose model.

without the need to derive specific damage parameter for each one of them. This simplicity, has led to its wide adoption for dose calculations in thermal therapy applications[9,10,12–14]. The current CEM_{43} model was originally developed for traditional hyperthermia applications (temperatures less than 47°C). The validity and accuracy of this model for high temperature applications (50–90°C) is questionable. This is demonstrated using *in-vivo* time-temperature data from Moritz and Henriques[2,3]. Each time-temperature combination yielded the same tissue damage, yet the doses using the current CEM_{43} model are different, most notably above 55°C where the dose increases rapidly with temperature as shown in figure 1.3.

Therefore, it is hypothesized that *the current CEM_{43} dose model over-estimates the accumulation of thermal damage for high-temperature thermal therapy applications, and a more accurate thermal dose model can be introduced based on experimental results and the rate process analysis.* A new CEM_{43} dose model is introduced in the next chapter. The new

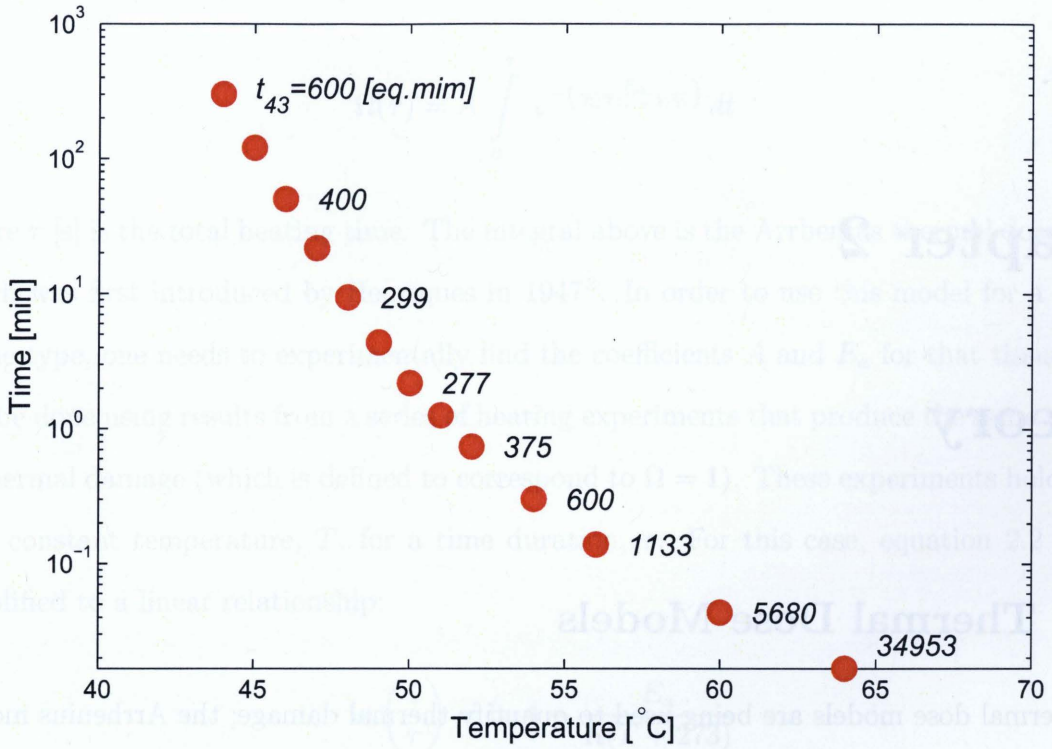

Figure 1.3: Time-temperature combinations resulting in an isothermal effect. The numbers represent the t_{43} dose values, in equivalent minutes, corresponds to each of these combinations. Ideally, the numbers should be very close which is not the case here.

model uses the same concept of equivalent minutes at 43°C. Though, the time-temperature relationship upon which the new dose calculation is based was derived by fitting experimental results of different biological systems over a wide range of temperatures (up to 70°C), as opposed to the "rule of thumb" approximation that is used in the current CEM_{43} model.

Chapter 2

Theory

2.1 Thermal Dose Models

Two thermal dose models are being used to quantify thermal damage; the Arrhenius model and the CEM_{43} model. These two models were introduced in the Chapter 1. In this section, the theory and the formulae for these models are presented. In Addition, a third dose model using Vogel-Tammann-Fulcher equation (VTF) to describe thermal damage processes, is introduced here.

2.1.1 Arrhenius model

Thermal damage has been modelled as a first-order rate process in which tissue constituents transform from native state to damaged state with a reaction velocity (or rate constant), k $[s^{-1}]$[3,22]. The dependence of k on temperature, as in many other reactions, can be described by the Arrhenius equation:

$$k = A\, e^{-\left(\frac{E_a}{R(T+273)}\right)} \tag{2.1}$$

where A is a frequency factor $[s^{-1}]$, E_a is the activation energy [J $mole^{-1}$], R the universal gas constant [8.23 J $mole^{-1}K^{-1}$], and T is the Temperature [°C]. Based on a first-order rate process assumption, accumulated thermal damage due to heating can be quantified by a

dimensionless parameter Ω:

$$\Omega(\tau) = A \int_0^{\tau} e^{-\left(\frac{E_a}{R(T(t)+273)}\right)} dt \tag{2.2}$$

where τ [s] is the total heating time. The integral above is the Arrhenius thermal dose model which was first introduced by Henriques in 1947[3]. In order to use this model for a certain tissue type, one needs to experimentally find the coefficients A and E_a for that tissue. This can be done using results from a series of heating experiments that produce the same amount of thermal damage (which is defined to correspond to $\Omega = 1$). These experiments hold tissue at a constant temperature, T, for a time duration, τ. For this case, equation 2.2 can be simplified to a linear relationship:

$$\ln\left(\frac{1}{\tau}\right) = \ln A - \frac{E_a}{R(T+273)} \tag{2.3}$$

A plot of $\frac{1}{(T+273)}$ versus $\ln(\frac{1}{\tau})$, known as an Arrhenius plot, should be a straight line (since E_a is constant parameter). The activation energy, E_a, can be found from the slope of the plot, while A can be found from its y-intercept.

2.1.2 CEM_{43} model

Sapareto and Dewey introduced a thermal dose model that uses the exposure time at 43°C to quantify thermal damage[5]. The model is usually called CEM_{43} (Cumulative Equivalent Minutes at 43°C). The dose in CEM_{43} is represented symbolically using t_{43} . Exposure at different temperatures is converted to t_{43} , which has the units of *equivalent minutes* at 43°C, using a simple time-temperature relationship. The accumulative dose value, in [eq.min], can be mathematically describe as:

$$t_{43} = \int_0^{\tau} C^{(43-T(t))}\, dt \qquad C = \begin{cases} 0.25 & T < 43°\text{C} \\ 0.5 & T \geq 43°\text{C} \end{cases} . \tag{2.4}$$

2.1.3 VTF model

For many temperature dependent reactions, a modified Arrhenius equations are used when the basic Arrhenius equation (2.1) does not describe the experimental data well. A modified Arrhenius-type asymptotic exponential equation, known as Vogel-Tammann-Fulcher equation (VTF) has been successfully applied to various rate processes[27–29]. In the VTF equation, the reaction velocity k has the following form[28,29]:

$$k = \begin{cases} A\, e^{-\left(\frac{a}{T-T_0}\right)} & T > T_0 \\ 0 & T \leq T_0 \end{cases} \tag{2.5}$$

where A [s^{-1}] is a frequency factor , a [K] is a parameter related to a dependent activation energy[29], T_0 [°C] is the absolute temperature where the dynamics of the given system can no longer be thermally activated[27,28], and T [°C] is the system temperature. T_0 is a system-based temperature that replaces the absolute zero (-273°C) in the basic Arrhenius equation. Hence, one can think of VTF equation as the general case of the basic Arrhenius equation. Using this modified Arrhenius equation, the thermal dose model in equation 2.2 becomes:

$$\Omega(\tau) = A \int_0^{\tau} e^{-\left(\frac{a}{T(t)-T_0}\right)}\, dt \tag{2.6}$$

By using the same assumptions and procedure to generate equation 2.3, one can generate a VTF analogue dependent on two parameters a, and A:

$$\ln\left(\frac{1}{\tau}\right) = \ln A - \frac{a}{T - T_0}. \tag{2.7}$$

By plotting $\frac{1}{(T-T_0)}$ versus $\ln(\frac{1}{\tau})$ one can find a and A from the plots using the slope and the y-intercept, respectively.

2.2 New CEM_{43} Model

Because of the simplicity and the universality of the CEM_{43} dose calculations, the goal of this work is to introduce a new more robust CEM_{43} dose model that improves the current one by making it applicable to a wider range of temperature. The new model uses the same units of equivalent minutes at 43°C to quantify thermal damage. This was done by linking the CEM_{43} to the Arrhenius model and fitting experimental data base on both Arrhenius and VTF equations.

The universality of the CEM_{43} dose model does not mean that all biological systems have the same time-temperature relation to achieve an isothermal effect. Rather, it assumes that they have parallel time-temperature relations. The current CEM_{43} model assumes that time-temperature relations to achieve an isothermal effect in all biological systems have a break at 43°C. This assumption of parallel relations means that the *normalized time* (relative to the time at some reference temperature, 43°C in this case) for all biological systems has the same relation with temperature to achieve an isothermal effect. That is, for the current CEM_{43} model if one heats tissue at constant temperature, T, for a period of time, τ, to achieve some thermal effect, then the amount of time one needs when heating at 43°C, t_{43} , to achieve the same effect is:

$$t_{43} = C^{(43-T)}\,\tau. \tag{2.8}$$

The natural logarithm of the *normalized time* (t_{43}/τ) then has a linear dependence on temperature:

$$\ln\left(\frac{t_{43}}{\tau}\right) = \ln(C)(43-T) \quad \text{or} \quad \ln\left(\frac{t_{43}}{\tau}\right) = \begin{cases} 1.4T - 60 & T < 43°\text{C} \\ 0.7T - 30 & T \geq 43°\text{C} \end{cases}. \tag{2.9}$$

Verification that *normalized* time (to time at 43°C) has the same relation with temperature to achieve isothermal effect in different biological systems was investigated using published experiment results (figure 2.1) . The goal, therefore, was to find a function $B(T)$

for which

$$\ln\left(\frac{t_{43}}{\tau}\right) = B(T) \tag{2.10}$$

was valid for different tissue types. If such a function exists and it fits the experimental data better than equation 2.9, it will be used to develop a new CEM_{43} model.

Four published data sets from four different experiments were considered. Each of them provides the exposure time, τ, at different constant temperatures, T, to achieve a certain isothermal effect. Three of the experiments were done *in vitro* by different groups and reported by Henle and Dethlefsen[26]. The fourth was done *in vivo* by Moritz and Henriques. The threshold, or the isothermal effect, in the fourth experiment was irreversible epidermal injury[2,3]. Since this experiment starts at 44°C, the time at 43°C was extrapolated from the other data points. The other three sets have 43°C as one of the temperatures. The *normalized* exposure time (t_{43}/τ) for each experiment was plotted against temperature, all in one semi-log plot shown in figure 2.1.

The relation between the *normalized time* (t_{43}/τ) and the heating temperature, T, to achieve an isothermal effect was derived based on both Arrhenius and VTF equations to find a general form for $B(T)$ in equation 2.10. Based on the Arrhenius model, for constant temperature of 43°C equation 2.3 becomes:

$$\ln\left(\frac{1}{t_{43}}\right) = \ln A - \frac{E_a}{R(43+273)} \tag{2.11}$$

Subtracting equation 2.11 from equation 2.3 gives:

$$\ln\left(\frac{t_{43}}{\tau}\right) = \frac{E_a}{R}\left(\frac{1}{43+273} - \frac{1}{T+273}\right) \tag{2.12}$$

This equation can be rewritten as:

$$\ln\left(\frac{t_{43}}{\tau}\right) = \frac{E_a}{R(43+273)}\,\frac{T-43}{(T+273)} \tag{2.13}$$

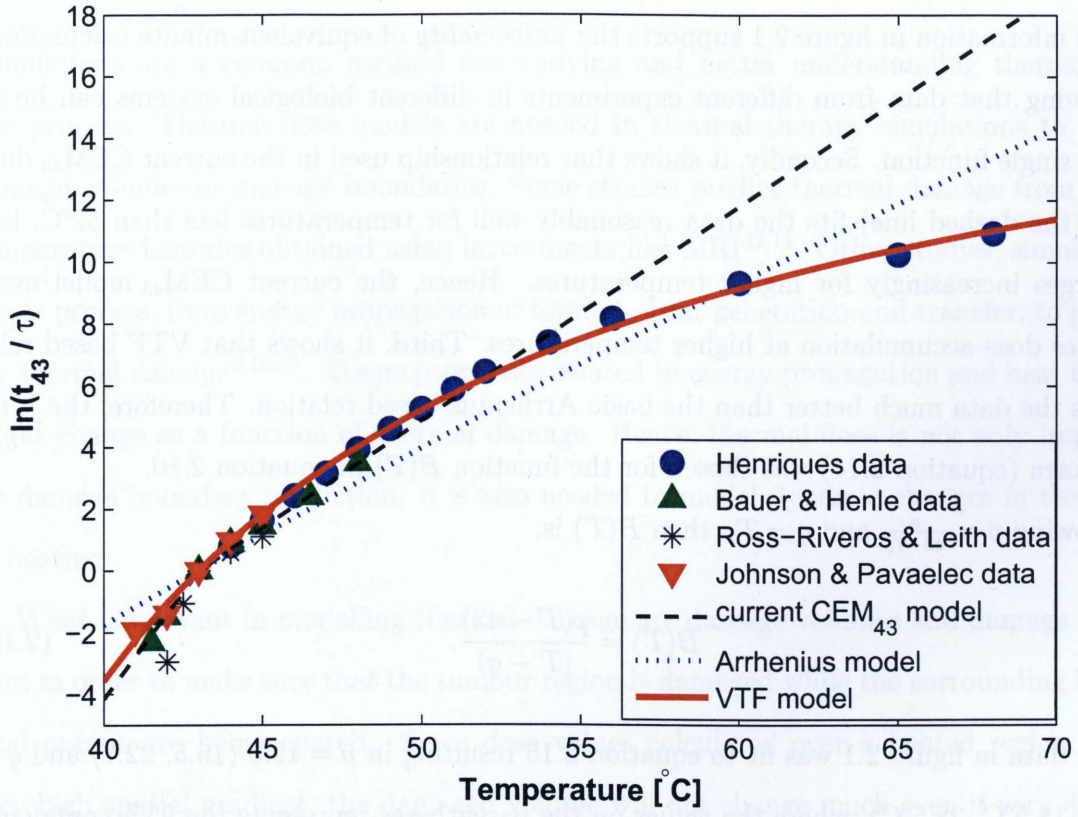

Figure 2.1: *Normalized time*-temperature relationship for different experimental data. The doted line is the fit based on Arrhenius equation, the solid red line is a fit based on VTF equation, while the dashed line is the relation on which the current CEM_{43} model based.

where τ is the heating time at an arbitrary constant temperature, T, to achieve some thermal effect (defined to correspond to $\Omega = 1$) which can also be achieved by heating at the constant temperature of 43°C for a period of time t_{43} . The experimental data in figure 2.1 was fit to equation 2.13 to find a value for the parameter $\frac{E_a}{R(43+273)}$. The fit is represented by the blue doted line in figure 2.1.

A relation similar to that in equation 2.13 can be derived using equation 2.7 from the VTF model:

$$\ln\left(\frac{t_{43}}{\tau}\right) = \frac{a}{43 - T_0}\frac{T - 43}{(T - T_0)}. \tag{2.14}$$

The same data was fitted to equation 2.14 to find the values for the two parameter T_0 and

$\frac{a}{43-T_0}$. The fit is represented by the red solid line in figure 2.1.

The information in figure 2.1 supports the *universality* of equivalent-minute calculations by showing that data from different experiments in different biological systems can be fit using a single function. Secondly, it shows that relationship used in the current CEM_{43} dose model (the dashed line) fits the data reasonably well for temperatures less than 52°C, but it diverges increasingly for higher temperatures. Hence, the current CEM_{43} model overestimates dose accumulation at higher temperatures. Third, it shows that VTF based relation fits the data much better than the basic Arrhenius based relation. Therefore, the VTF based form (equation 2.14) was chosen for the function $B(T)$ in equation 2.10.

Allowing $p = \frac{a}{43-T_0}$ and $q = T_0$, then $B(T)$ is:

$$B(T) = \frac{p(T-43)}{(T-q)}. \tag{2.15}$$

The data in figure 2.1 was fit to equation 2.15 resulting in $p = 19.6$ (16.5, 22.7) and $q =$ 23.5°C (18.5°C, 28.5°C), where the values on the parentheses represents the 95% confidence bounds, and the goodness of fit was $R^2 = 0.99$. Substituting equation 2.15 into equation 2.10 produces a new CEM_{43} dose model:

$$t'_{43} = \int_0^{\tau} e^{\left(\frac{p(T(t)-43)}{T(t)-q}\right)} dt. \tag{2.16}$$

The next chapter presents results from testing the ability of this new model in predicting thermal damage compared to the current CEM_{43} model. The investigations were done using both constant-temperature and time varying temperature experiments. The applicability of VTF model, with $T_0 = q$ =23.5°C compared to the basic Arrhenius model in thermal damage applications is also shown in the next chapter. The results of LITT simulations are shown as well to investigate the deviation between t_{43} and t'_{43} in predicting damaged volume. Before this, the theory of LITT modelling is described in the following section.

2.3 Theory of LITT Modelling

Simulations are a common method for studying and better understanding thermal therapy process. Thermal dose models are needed in thermal therapy simulations to predict damage volumes or damage boundaries. Some studies predict thermal damage from spatial temperature-histories obtained using instruments like MRI[12,14]. Other studies, simulate the whole process, from energy propagation in tissue to heat generation and transfer, to predicting thermal damage[9,10,30]. Tissue properties related to energy propagation and heat transfer might change as a function of thermal damage. Hence, thermal dose is not only important for damage boundary prediction, it is also needed to model dynamic changes in tissue due to heating.

What is relevant in modelling thermal damage are damage volumes and damage boundaries in order to make sure that the tumour region is damaged while the surrounding healthy vital organs are being spared. Since dose values calculated over a heated region have a very high spatial gradient, the damaged volume will not change much even if very different threshold dose values are used. Therefore, the predicted volume of damage using t_{43} versus t'_{43} might be similar. A theoretical model for laser interstitial thermal therapy (LITT) in prostate was built to investigate this.

LITT is a minimally invasive technique for destroying localized solid tumours. Laser energy is applied directly to the tumour region via one or more flexible optical fibres inserted into the tissue. The objective of LITT is to achieve irreversible thermal damage in a targeted tumour region over a period of a few minutes while saving the surrounding healthy tissues and vital organs. A finite-element LITT simulation was developed using the COMSOL Multiphysics© (COMSOL AB, Stockholm).

LITT is a complex process that involves many physical variables that change non-linearly during the treatment as shown in figure 2.2. The modelling of this process can be broken up into optical diffusion, heat transfer and thermal damage. Each of these is described below.

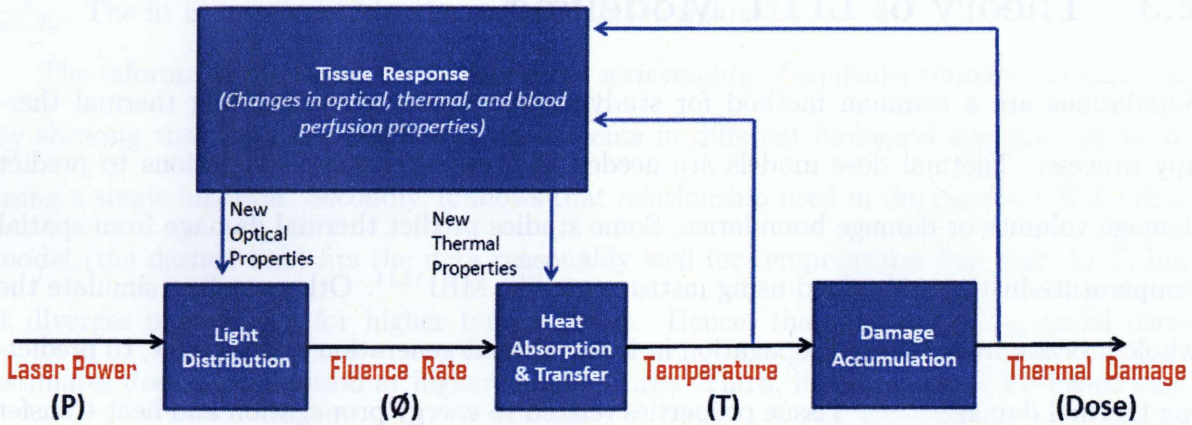

Figure 2.2: Schematic of physics and modelling of the laser interstitial thermal therapy. fluence rate, temperatures rise, and thermal damage can be modelled. Tissue properties change during heating which makes LITT non-linear process.

2.3.1 Model geometry

A 2-D axisymmetric geometry was used, with rotational symmetry around the axes of the fibre, in which laser energy diffuses only through the sides of a 2 cm diffuser (boundary # 1 in figure 2.3). The boundaries of the computational domain were far enough from the centre of the source (5 cm) such that no changes occur at them. The mesh in figure 2.3 has 44,502 elements. The number of degrees of freedom for the coupled problem was 244,035. A 10 minutes LITT treatment, simulated using COMSOL Multiphysics©, takes 18.4 minutes to solve and uses 8GB of RAM.

2.3.2 Optical diffusion

Because of the high scattering nature of tissue, the diffusion approximation of radiative transport equation can be used to model light distribution in tissue[31,32]:

$$\nabla \cdot (-D_c \nabla \phi(\mathbf{r})) + \mu_a \phi(\mathbf{r}) = S(\mathbf{r}) \tag{2.17}$$

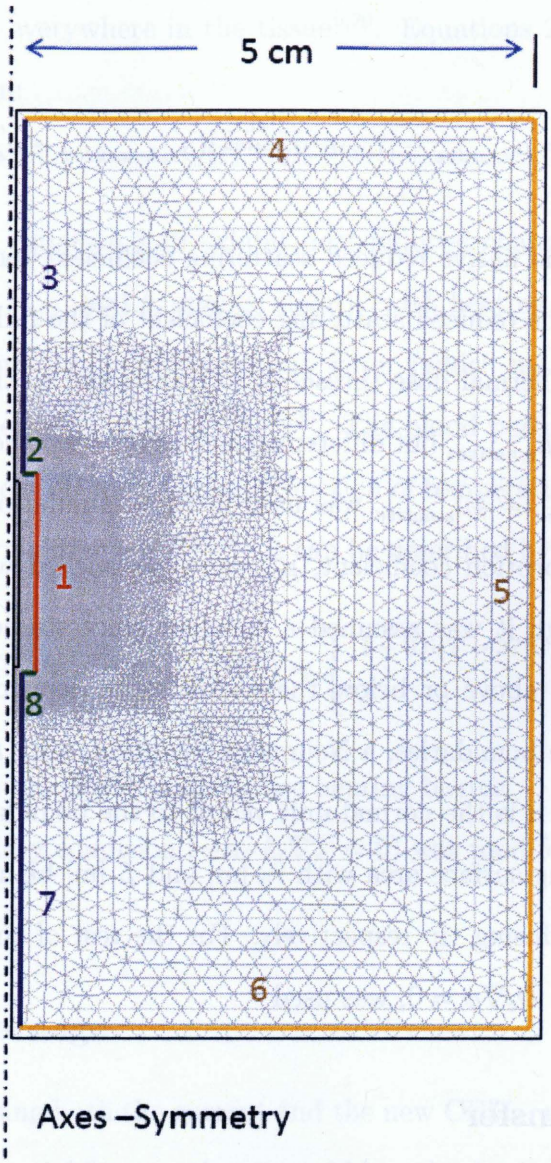

Figure 2.3: Geometry and finite-element mesh of the 2-D axisymmetric LITT model. Numbered thicker line inside were added for clarification. Boundary # 1 is the surface of the diffusing fibre.

where $D_c = 1/[3(\mu_a + \mu_s')]$ [m] is the diffusion coefficient, μ_a [m^{-1}] is the optical absorption coefficient, μ_s' [m^{-1}]is the reduced scattering coefficient, ϕ [W m^{-2}] is the optical fluence rate, $\mathbf{r}$ [m] is position vector, and S [W m^{-3}] is the absorbed power density. The reduced scattering coefficient changes during the treatment as a function of thermal dose as shown

in following equation[9]:

$$\mu_s'(t_{43}) = \mu_{s\_native}' + [1 - e^{\frac{-t_{43}}{t_{43\_critical}}}](\mu_{s\_denatured}' - \mu_{s\_native}') \tag{2.18}$$

where μ_{s_native}' [m^{-1}] is the native reduced scattering coefficient for the tissue before heating, $\mu_{s\_denatured}'$ [m^{-1}] is the reduced scattering coefficient of the fully denatured tissue, and $t_{43\_critical}$ [eq.min] is the thermal dose threshold corresponding to the onset of the damage. $\mu_{s\_denatured}'$ is higher than μ_{s_native}', but different relations between these two values have been reported.[4,33,34]. $\mu_{s\_denatured}' = 4\mu_{s\_native}'$ was used in these simulations based on a paper by Skinner *et al*[4]. The absorption coefficient, μ_a, can be modelled with an equation similar to equation 2.18, although it was assumed a constant since studies show that it changes slightly with coagulation above or below the native value depending on tissue type and wavelength[4,33,34]. For the boundaries, a Neumann condition, $-\mathbf{n} \cdot D_c \nabla\phi = \frac{P}{2\pi r_0 L}$, was used at boundary # 1 , where $\mathbf{n}$ is the normal unit vector to the boundary, P is the laser power [W], $2\pi r_0 L$ is the diffusing surface area with r_0 [m] and L [m] being the radius of the fibre and the length of the diffusing tip respectively. For the rest of the boundaries (2–8), the Neumann condition, $-\mathbf{n} \cdot D_c \nabla\phi = 0$, was used.

2.3.3 Bioheat transfer

Heat is generated in the tissue region due to absorption of light and then propagates through the tissue. This can be described using the Pennes bioheat equation[35],

$$\rho_t c_t \frac{\partial T}{\partial t} = \nabla \cdot (k_t \nabla T(\mathbf{r}, t)) + Q(\mathbf{r}) - \omega_b c_b (T(\mathbf{r}, t) - T_b) \tag{2.19}$$

where T is tissue temperature [°C], t is time [s], ρ_t, c_t, and k_t are density [kg m^{-3}], specific heat [J kg^{-1} K^{-1}], and thermal conductivity [W m^{-1} K^{-1}] of tissue respectively. While, ω_b [kg m^{-3} s^{-1}], c_b [J kg^{-1} K^{-1}], and T_b are the blood perfusion rate, blood specific heat, and blood temperature (37°C), respectively. Q is the heat source [W m^{-3}] which is related to the

absorbed optical energy everywhere in the tissue[9,20]. Equations 2.17 and 2.19 are coupled by the following equation:

$$Q(\mathbf{r}) = \mu_a \, \phi(\mathbf{r}). \tag{2.20}$$

The tissue properties in equation 2.19 exhibit heat-induced changes during the treatment. The thermal properties, ρ_t c_t, and k_t change slightly with heating. They can reasonably be assumed to have the same dynamic changes as water (which makes up 83% for prostate) thermal properties in the range of 20–100°C[20,36]. The blood perfusion rate changes significantly during the treatment. It increases as a function of temperature and decreases to reach zero as a function of thermal damage[30,37,38]. It can be described by the following equation[38]:

$$\omega_b(T, t_{43}) = \omega_{b0} \, f(T) \, e^{\frac{-t_{43}}{t_{43\_critical}}} \qquad f(T) = \begin{cases} 1 + 0.6(T - 37°\text{C}) & T < 42°\text{C} \\ 4 & T \geq 42°\text{C} \end{cases} \tag{2.21}$$

where ω_{b0} is the baseline blood perfusion before heating begins.

The Neumann boundary condition ($-\mathbf{n} \cdot k_t \nabla T = 0$) was used for all boundaries (1–8) in the thermal model.

2.3.4 Thermal damage

Simulations were done using both the current and the new CEM_{43} models. Equation 2.4 was reformulated into a differential form so that it could be solved using the finite-element based software COMSOL Multiphysics©:

$$\frac{dt_{43}}{dt} = C^{(43 - T(\mathbf{r},t))} \tag{2.22}$$

The same thing was done for the new CEM_{43} model from equation 2.16:

$$\frac{dt'_{43}}{dt} = e^{\frac{p(T(t)-43)}{(T(t)-q)}} \tag{2.23}$$

Equations 2.17, 2.19, and 2.22 or 2.23 are coupled, and were solved using COMSOL Multiphysics© as a coupled system. Unless mentioned above, all prostate tissue properties and other constants in the above equations were adopted from the thesis by Madhu Jain[20].

Chapter 3

Results

3.1 CEM_{43} models Results

3.1.1 Epidermal injury

In their work titled "Studies of thermal injury" in 1947, Moritz and Henriques tried to find information about the rate at which skin burning occurred at any given surface temperature. They gained time-temperature thresholds resulting in different levels of skin injuries. They did their experiments *in vivo* for both porcine and human skin. Experiments were done at constant temperatures. The skin surface was immediately brought and maintained at a predetermined constant temperature using an applicator by which a running stream of temperature-controlled water was brought in direct contact with the skin[2]. In introducing the Arrhenius based dose calculations, Henriques used two of the epidermal injury thresholds: "threshold A" and "threshold B"[3]. Threshold A was used to produce one of the data sets used in figure 2.1. This threshold represents the minimum exposure time resulting in complete transepidermal necrosis. Threshold B represents the maximum exposure time resulting in reversible epidermal injury. This threshold was used to produce the data used in figure 1.3 to show the inconsistency in the current CEM_{43} dose model. Since the time-temperature combinations in threshold B results in an isothermal effect, an ideal thermal dose model

should predict the same dose value for each combination.

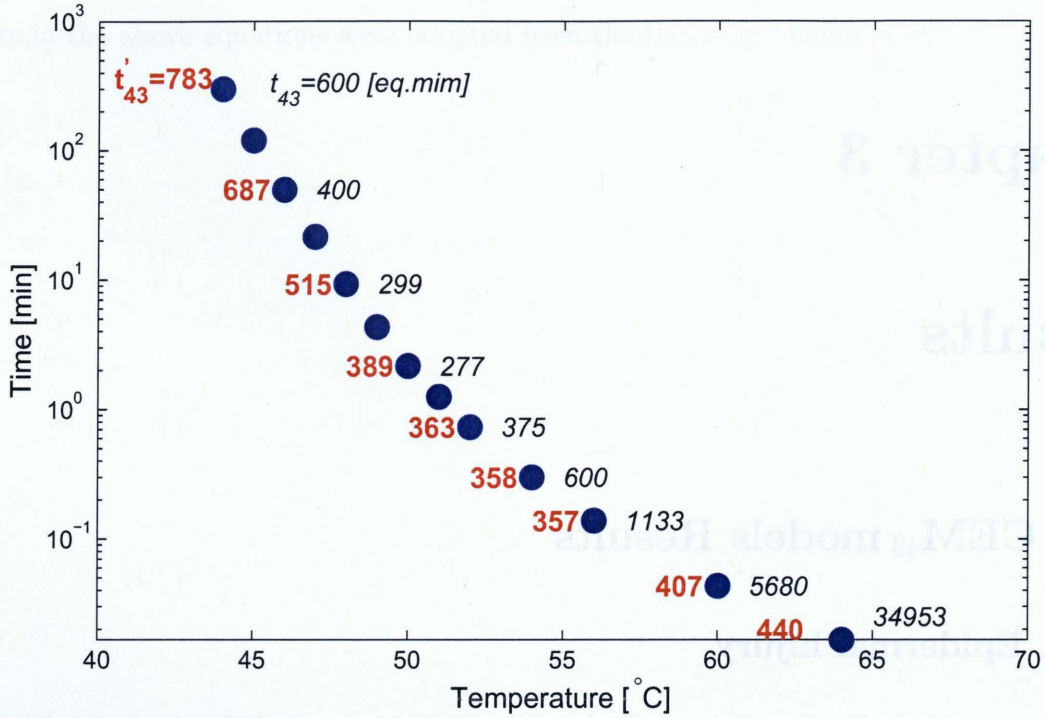

Figure 3.1: Time-temperature combinations resulting in an isothermal effect; maximum exposure time produces reversible epidermal injury[2,3]. The numbers on the left represent the t'_{43} dose values in equivalent minutes and the ones on the right represent the t_{43} dose values.

Figure 3.1 repeats the results previously shown in figure 1.3 and adds t'_{43} dose values on the left side of the data-points. The t'_{43} dose values are in the same order of magnitude and are more consistent than the t_{43} dose values which has 2 orders of magnitude difference for high temperatures. This gives an indication that the new CEM_{43} model is more consistent in predicting thermal damage than the current CEM_{43} model.

3.1.2 Thermal damage in cartilage

Studying cell viability and finding survival fraction after heat exposure is a common experiment in thermal dosimetry studies. Survival information, which shows survival fraction versus exposure time for different constant temperatures were used for quantifying thermal

damage[5,24,26,39,40]. Thermal damage increases as survival fraction decreases. An ideal thermal dose model should predict a unique dose value for a distinct survival fraction. The new dose model was tested using detailed survival information from a study using a relatively high range of temperatures (48°C–62°C)[40]. The study characterized cellular damage due to heating in rabbit nasal cartilage by quantifying the concentration of healthy cells (the surviving fraction) in tissue samples versus exposure time at constant temperature water baths (48–62°C). For each time-temperature combination, the dose value in equivalent-minutes was calculated using both the current CEM_{43} model and our new CEM_{43} model. Since the surviving fraction for each of these combinations is given, the dose survival response for both models were plotted as shown in figure 3.2.

Looking at figure 3.2, two things are noticed. The t_{43} dose values (in parts a and b) are very high in comparison to the t'_{43} dose values (in parts c and d), although both of them are based on the same time-temperature information. More importantly, the survival-t'_{43} response is closer to the ideal survival-dose relation, where a distinct survival fraction is mapped to a unique dose value, than the survival-t_{43} response where the survival lines do not join each other, and the same surviving fraction corresponds to a wide range of t_{43} values. This shows that the new CEM_{43} model is more consistent in predicting thermal damage than the current one. The new model is closer to an ideal thermal dose model than the current one.

3.1.3 Laser-induced heating

All the data used in deriving the dose model and the testing thus far were from controlled experiments where heating takes place at constant temperatures. Thermal dose models are needed for clinical applications like cancer where temperatures vary throughout the tissue and change with time. Hence, we need to look at dose prediction results in real transient heating experiments similar to those in thermal coagulation treatments. Data from *ex-vivo* liver heating experiments obtained from UPEI were used for this purpose[41].

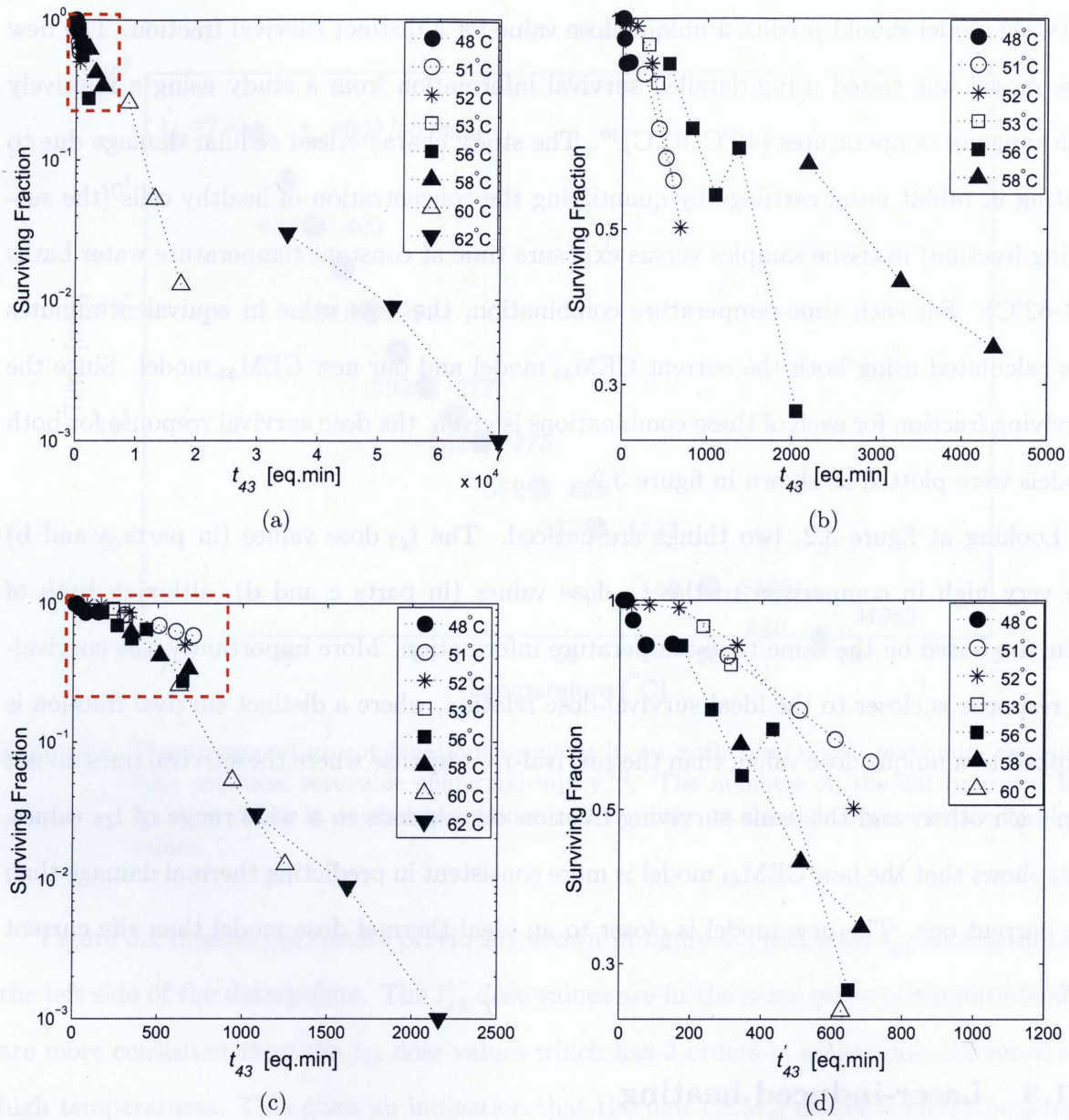

Figure 3.2: The dose survival response using t_{43} model in (a), (b) shows the details of the framed region in (a). The dose survival response using t'_{43} similarly shown (C) and (d).

In each of these experiments, six thermal lesions were created on the surface of an adult bovine liver sample using laser energy. A multimode optical fibre with a 1 mm core diameter and 0.37 numerical aperture (ThorLabs, Newton, NJ, USA), coupled to a Diomed 60, 810 nm diode laser (Diomed, Cambridge, UK) was placed 13 mm away from the tissue surface.

Constant laser power of 1.3–1.6W for 1–6 minutes exposure time was used to produce the lesions. Each lesion has a 1 minute longer exposure time than the previous one. This caused different lesion sizes and different temperature histories . Surface temperature history for each lesion was collected using a thermal camera (FLIR ThermaCAM SC2000, FLIR Systems, Burlington, On, Canada) with a 34/80 close-up lens at a rate of one frame per second. The sample was originally frozen, and was brought quickly to room temperature before the start of the experiment. The tissue was allowed to cool to room temperature after the creation of each lesion. The thermal camera continued to collect data two minutes after the laser was turned off. After the lesions were created, an optical image of the sample was acquired and is shown in figure 3.3a.

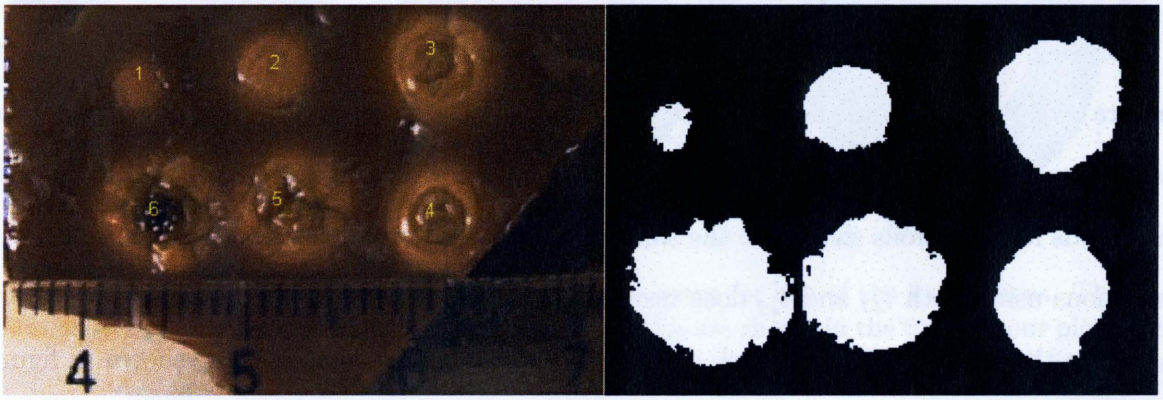

(a) (b)

Figure 3.3: Six lesions generated in bovine liver using laser with different heating time in (a). The degree of tissue whitening is related to the severity of thermal damage, hence, the borders of the lesions in the binary image in (b) correspond to the same amount of damage

Calculated t_{43} and t'_{43} doses were generated using the temperature data from the thermal camera and compared against the level of thermal damage. A 2 minute cool down period was included in the calculations since damage keeps accumulating after heating has stopped. Temperatures at the end of this period were observed to be too low to significantly accumulate more dose. The dose values in equivalent-minutes were calculated using both the current and the new CEM_{43} models. Although t_{43} values are clearly higher than the t'_{43} values, neither

this fact nor the values themselves can tell information about the validity or the superiority of any of the two models. They were each compared against a measure of thermal damage to test their predictions.

Since thermal damage in liver tissue is correlated with change in tissues optical properties or tissue whitening[4], an arbitrary brightness threshold (in the whitening range of lesions boundaries) was chosen for the image in figure 3.3a. This was done by converting the coloured image to a binary (black and white) image, and then choosing a certain image intensity (which corresponds to choosing a certain damage threshold) to create 6 white areas in the black background as shown in figure 3.3b. Then, the areas enclosed inside this threshold boundaries, were calculated. In this way, the surface areas of 6 lesions, all of them bounded by the same thermal damage contour, were obtained.

For each lesion, the calculated dose values (using the data obtained by the thermal camera) were used to find the dose threshold that would enclose the same area obtained for that lesion with the white light image processing as shown in figure 3.4 . Ideally the dose thresholds for all lesions should be the same. Figure 3.5 shows these threshold values for the six lesions using both t_{43} and t'_{43} dose results.

Using the current CEM_{43} model, dose threshold values for the 6 lesions, shown in figure 3.5a, have an average, $\mu = 3.4 \times 10^6$ eq.min, a standard deviation, $\sigma = 3.3 \times 10^6$ eq.min, and a coefficient of variation $C_v = \frac{\sigma}{\mu} = 0.99$. While using the new CEM_{43} model, the thresholds (figure 3.5b) have an average, $\mu = 3.0 \times 10^4$ eq.min, a standard deviation $\sigma = 1.1 \times 10^4$ eq.min, and a coefficient of variation $C_v = \frac{\sigma}{\mu} = 0.37$. Similar results were obtained when the same procedure was repeated for a second liver sample. For the second sample, the coefficient of variation using the current CEM_{43} ($C_v = 0.86$) was again higher than the one using the new CEM_{43} ($C_v = 0.40$). These results demonstrate the consistency of the new CEM_{43} dose model in predicting thermal damage in comparison with the current CEM_{43} dose model.

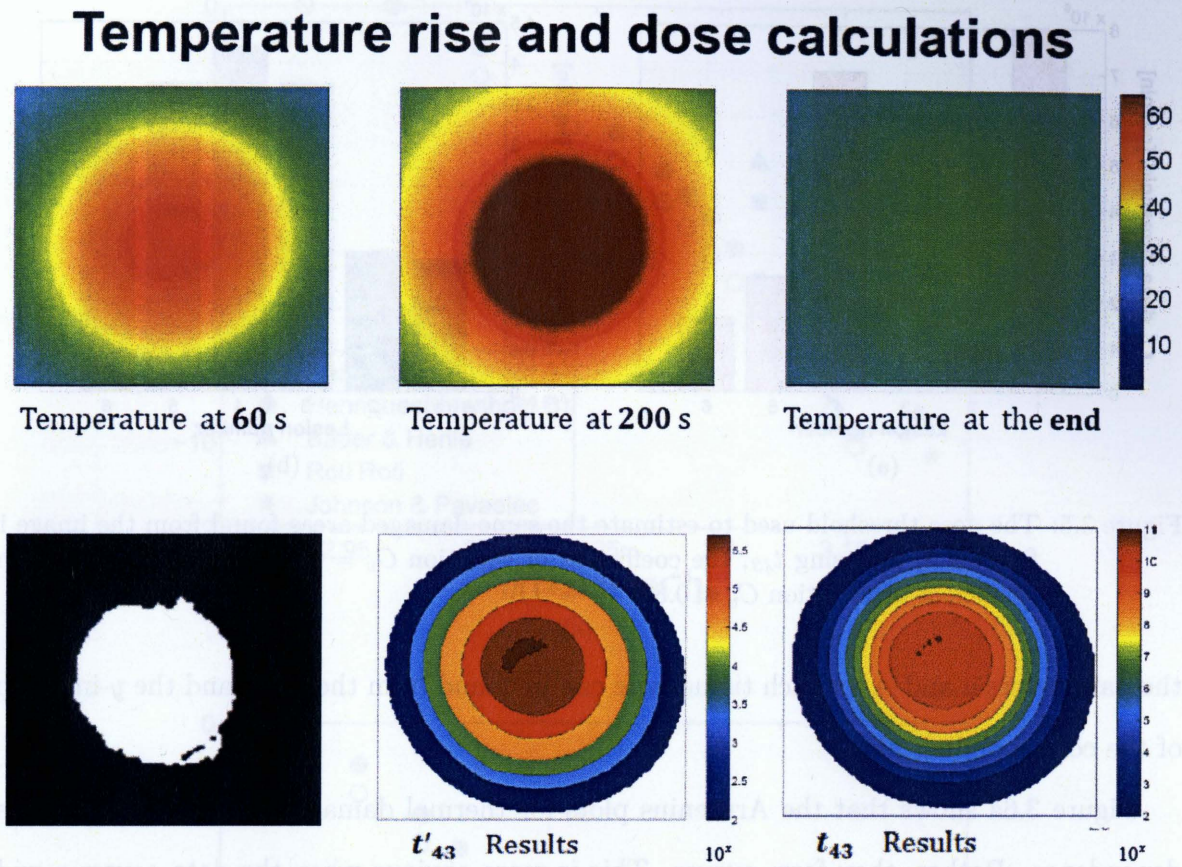

Figure 3.4: The top three images are the temperature maps for one of the liver lesions. The dose maps produced using new and current CEM_{43} are shown in the two contour plots. The dose thresholds in t'_{43} and t_{43} to enclose the same area in the lower left image was found.

3.2 Arrhenius and VTF Results

The Arrhenius plots(review section 2.1.1 for a description of Arrhenius plots) for the two damage thresholds A & B (described in section 3.1.1) from Moritz and Henriques[2,3], and of three other experiments reported in Henle *et al*[26] are shown in figure 3.6. Figure 3.6a is the Arrhenius plots of $\ln(1/\tau)$ versus $1/(T+273)$. According to equation 2.3, the plots should fit straight lines where the parameters E_a and A can be found for each type of tissue from its plot. Similarly, figure 3.6b shows a *modified* Arrhenius plots, using the VTF form, of $\ln(1/\tau)$ versus $1/(T-23.5)$. Based on equation 2.7, the plots should fit straight lines where

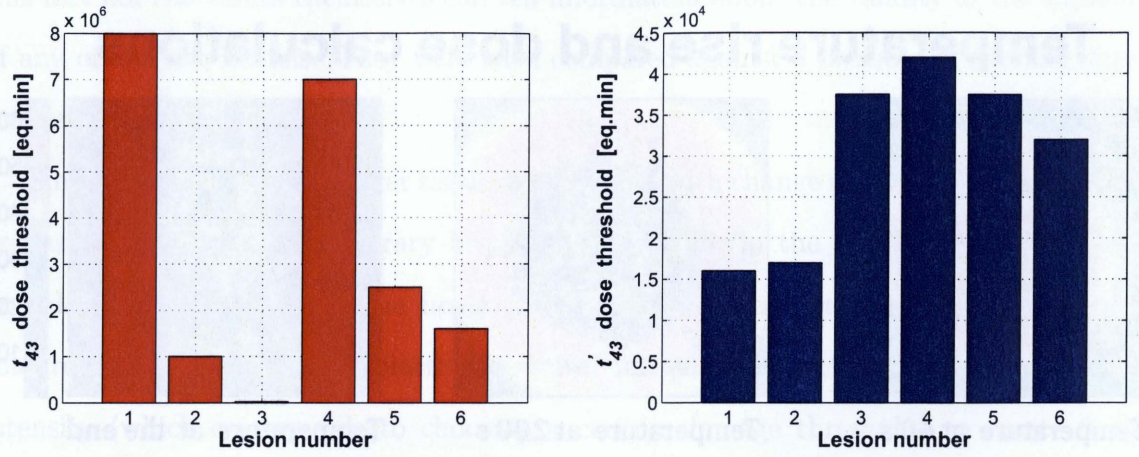

(a) (b)

Figure 3.5: The dose threshold used to estimate the same damaged areas found from the image in figure 3.3, (a) using t_{43}, the coefficient of variation $C_v = 0.99$, and (b) using t'_{43}, the coefficient of variation $C_v = 0.37$.

the parameters a and A for each tissue type can be found from the slope and the y-intercept of the corresponding plot.

Figure 3.6a shows that the Arrhenius plots for thermal damage do not exhibit a linear dependence. Rather, they form curves. This is more obvious when the data covers a wide range of temperatures. Constant values for the parameters E_a and A, assuming a linear Arrhenius plot, will produce a *poor* fit to the data. Hence, the basic Arrhenius model does not describe the kinetics of the thermal damage process very well. On the other hand, figure 3.6b shows that modified Arrhenius plots (using VTF model with $T_0 = 23.5$°C) are very close to straight lines. Constant values for the parameters a and A will produce a better fit to the data. Hence, the VTF equation appears to better describe the kinetics of the thermal damage process compare to the Arrhenius equation.

Henriques derived Arrhenius parameters (for thermal damage process in skin) by assigning $\Omega = 1$ for threshold A in the epidermal injury data[3]. He found that $\frac{E_a}{R} = 75000$ K and $A = 3.1 \times 10^{-98}$ s^{-1}. While using VTF equation for the same threshold, and assuming $\Omega = 1$, the parameters derived from figure 3.6b were $a = 393$ K and $A = 8.6 \times 10^{-3}$ s^{-1}. Calculated exposure times that correspond to $\Omega = 1$ using both models were plotted versus temperature

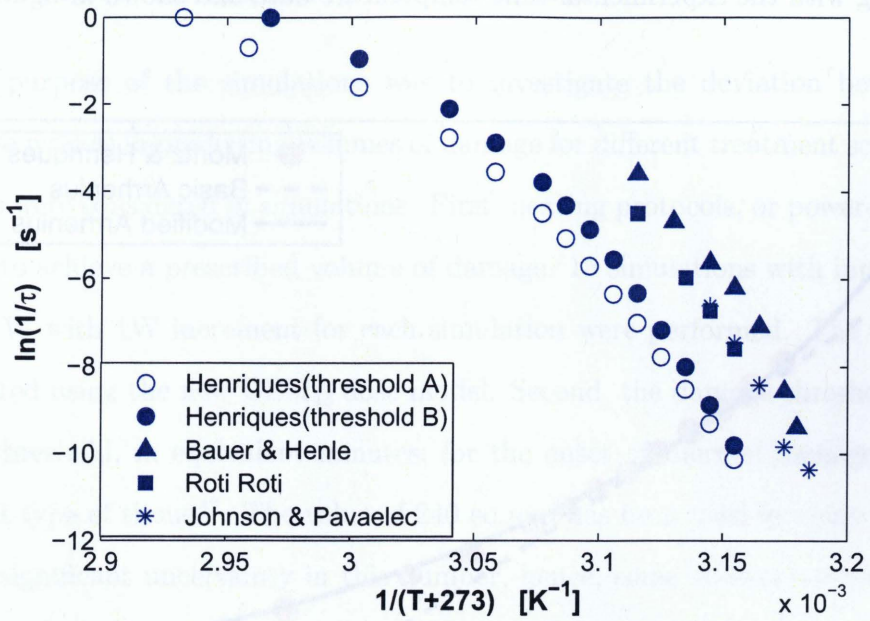

(a)

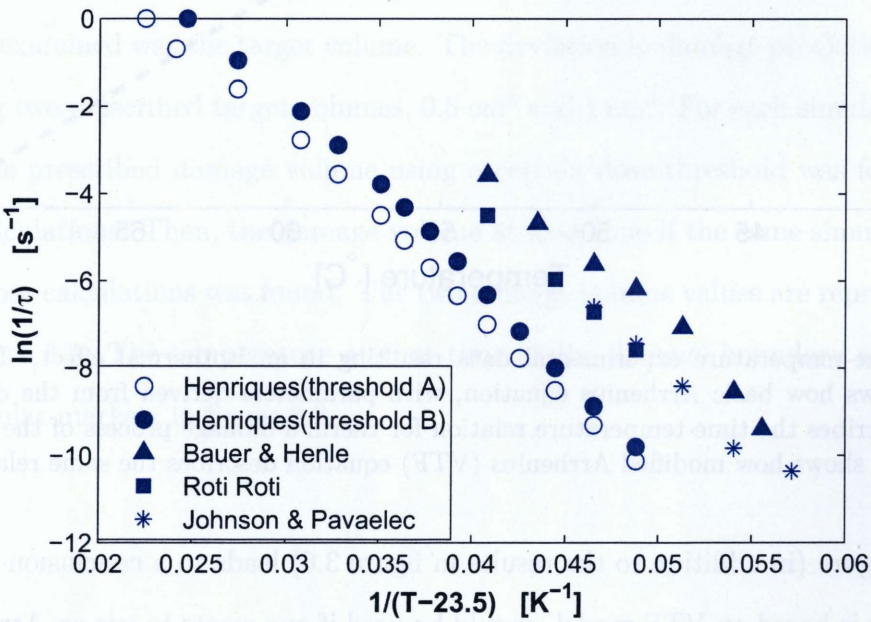

(b)

Figure 3.6: Arrhenius plots for different biological systems are shown in (a). In (b), the *modified* Arrhenius plots (using VTF model with $T_0 = 23.5°C$) are shown for the same biological systems.

(40–70°C) along with the experimental time-temperature data and shown in figure 3.7. The

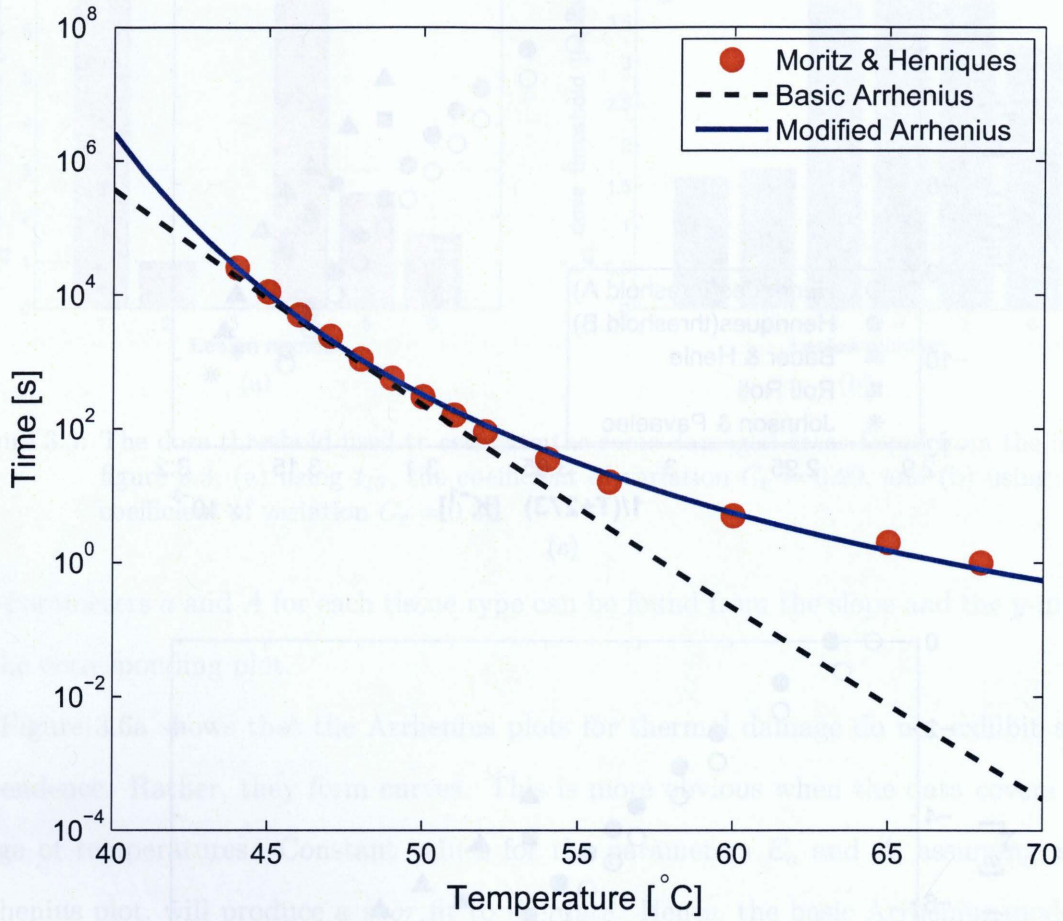

Figure 3.7: Time-temperature experimental data resulting in an isothermal effect. Dashed line shows how basic Arrhenius equation, with parameters derived from the data itself[3], describes the time-temperature relation for thermal damage process of the skin. Solid line shows how modified Arrhenius (VTF) equation describes the same relation.

result in the figure (in addition to the results in figure 3.6) leads to a conclusion that equation 2.6, which is based on VTF model, should be used if one wants to use an Arrhenius-like thermal dose model for specific type of tissue.

3.3 Results of LITT Simulations

The main purpose of the simulations was to investigate the deviation between the two CEM_{43} dose models in predicting volumes of damage for different treatment scenarios. Three parameters were considered in simulations. First, heating protocols, or power-time combinations used to achieve a prescribed volume of damage. 15 simulations with input laser power from 1–15 W with 1W increment for each simulation were performed. The 15 simulations were repeated using the new CEM_{43} dose model. Second, the damage threshold was varied. The dose threshold, in equivalent minutes, for the onset of thermal damage was reported for different type of tissue[42]. The value of 240 eq.min has been used in many studies[12–14,20]. There is s significant uncertainty in this number, hence, some studies considered a margin of 4 to 20 times this value in their investigations[12,13]. Two different threshold values, 240 eq.min and 5,000 eq.min, were considered and the results are shown in figure 3.8. The third parameter examined was the target volume. The deviation in damage prediction was investigated using two prescribed target volumes, 0.5 cm^3 and 1 cm^3. For each simulation, the time to reach the prescribed damage volume using a certain dose threshold was found based on t_{43} dose calculations. Then, the damage volume at that time if the same simulation was run using t'_{43} dose calculations was found. The two damage volume values are represented by the bars in figure 3.8. The temperature at that time at the damage boundary are represented by the circular markers in figure 3.8.

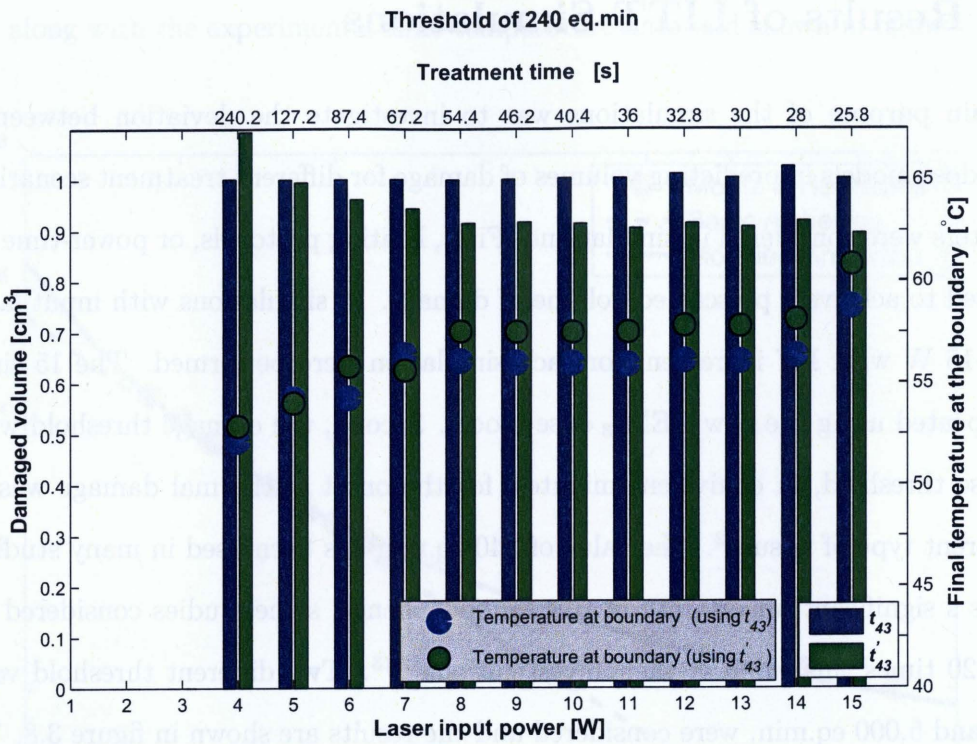
Threshold of 240 eq.min
Treatment time [s]
240.2 127.2 87.4 67.2 54.4 46.2 40.4 36 32.8 30 28 25.8
Damaged volume [cm3]
Final temperature at the boundary [°C]
Temperature at boundary (using t_{43})
Temperature at boundary (using t'_{43})
t_{43}
t'_{43}
Laser input power [W]

(a)

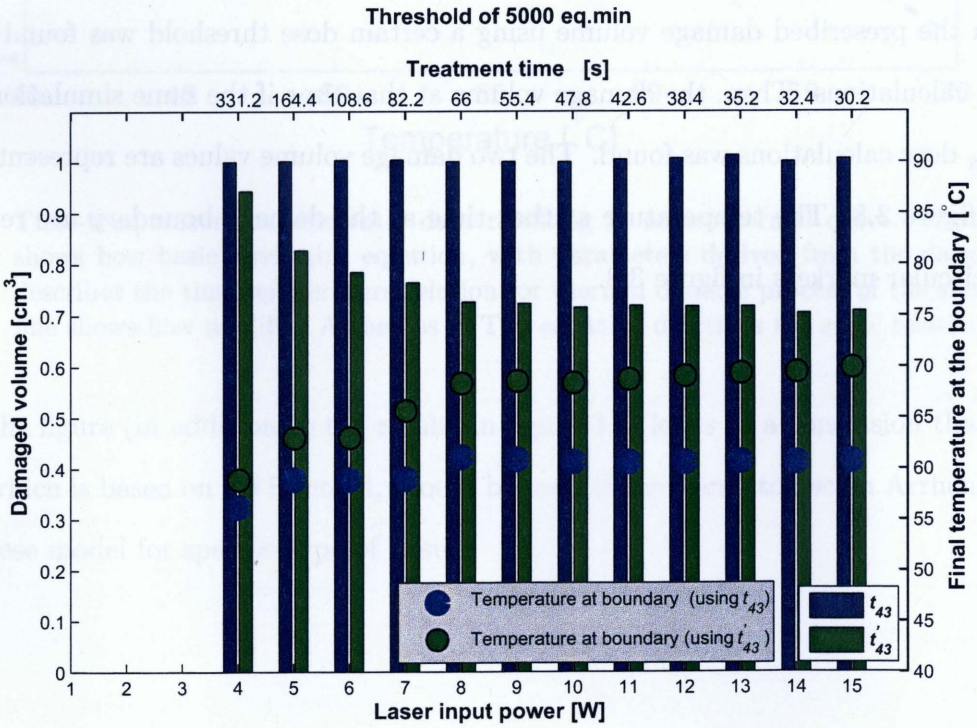
Threshold of 5000 eq.min
Treatment time [s]
331.2 164.4 108.6 82.2 66 55.4 47.8 42.6 38.4 35.2 32.4 30.2
Damaged volume [cm3]
Final temperature at the boundary [°C]
Temperature at boundary (using t_{43})
Temperature at boundary (using t'_{43})
t_{43}
t'_{43}
Laser input power [W]

(b)

Figure 3.8

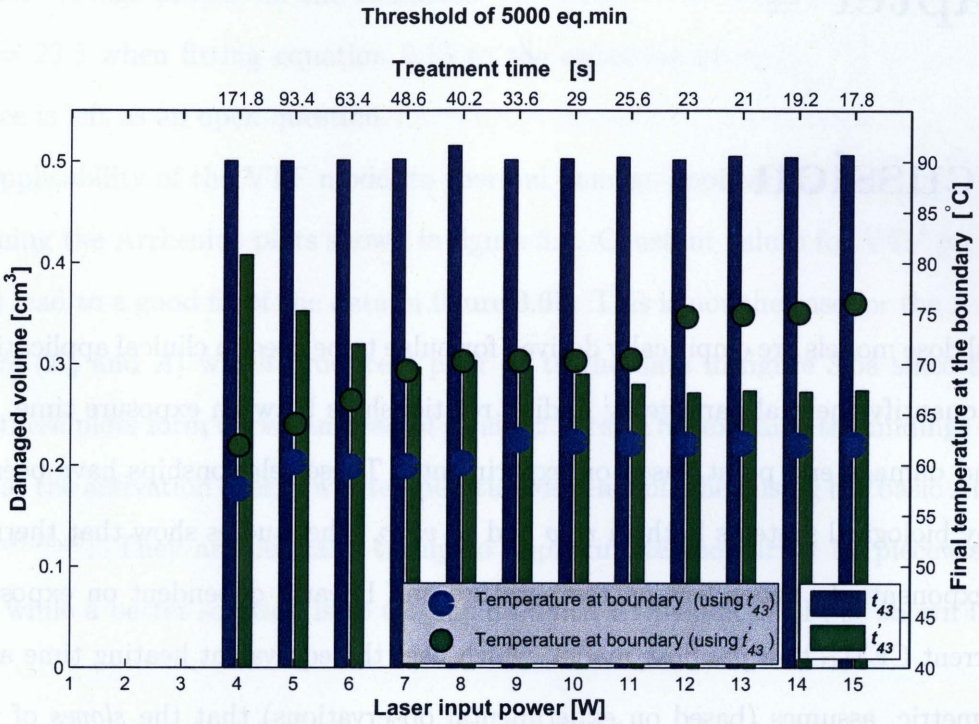

(c)

Figure 3.8: The results of 15, LITT, simulations using different laser power. In (a), the dark blue bars represent the closest damaged volume to a prescribed one of 1 cm^3 based on time stepping of the solution and using t_{43} and 240 eq.min as dose threshold , while the light green bars are the damaged volume at that same time step using t'_{43} in simulation. The time to reach the prescribed damage volume (the treatment time) is in top axes for each simulation. The blue and the green circular markers represent temperatures (right axes) at damage boundaries using the old and the new dose models at that moment respectively. (b) shows the same result using a dose threshold of 5,000 eq.min, and (c) using this same threshold but with a prescribed damaged volume of 1/2 cm^3.

Chapter 4

Discussion

Thermal dose models are empirically derived formulae to be used in clinical applications. The models quantify thermal damage by finding relationships between exposure time, temperature, and damage end point based on experiments. These relationships have been studied for many biological systems both *in vivo* and *in vitro*. The studies show that thermal damage is exponentially dependent on temperature and linearly dependent on exposure time. The current CEM_{43} thermal dose model, which uses the equivalent heating time at 43°C as a dose metric, assumes (based on experimental observations) that the *slopes* of the time-temperature relations to achieve an isothermal effect in all biological systems have a break at 43°C. The values of the slopes, above and below 43°C, are related to the two constant values of C in equation 2.4. While the value C should vary with temperature[5], the two values are a good approximation for traditional hyperthermia applications (temperatures less than 47°C). The validity of this approximation for high temperature applications (50 - 90°C) is questionable. Hence, a new time-temperature relation, to be used in a new CEM_{43} thermal dose model, is needed. The relation should have (in correspondence to a temperature-dependent C value) a continuously changing slope. This is the case of the new relation described by equation 2.15, as shown in figure 2.1.

A modified Arrhenius equation, the VTF equation, offers a better fit to experimental

data (figure 2.1) and was therefore used to develop the new CEM_{43} model. The VTF can be considered as a general form of the basic Arrhenius equation, in which there is an absolute temperature, T_0, below which the reaction can no longer be thermally activated[27–29]. This temperature is absolute zero (-273°C) in the basic Arrhenius case. The absolute temperature for thermal damage process in the examined experiments was close to room temperature ($T_0 = q = 23.5$ when fitting equation 2.15 to the experimental data). Whether this is a coincidence is left as an open question.

The applicability of the VTF model to thermal damage applications can be determined by examining the Arrhenius plots shown in figure 3.6. Constant values for VTF parameters (a and A) lead to a good fit of the data in figure 3.6b. This is not the case for the Arrhenius parameters (E_a and A) which produce a poor fit to the data in figure 3.6a since the data points in these plots form curves instead of straight lines. This explains the findings in some studies that the activation energy was temperature dependent when using the basic Arrhenius equation[6,24,25,43]. They are basically trying to approximate the curves by piecewise-linear relations, while a better solution is to use the modified Arrhenius, VTF, as shown in figure 3.6b.

It is important to note that using a universal CEM_{43} model for all tissue types is an approximation to using the VTF model for specific type of tissue. A universal CEM_{43} model assumes that all tissue types exhibit the same slope in the modified Arrhenius plots. Using $p = \frac{a}{43-23.5} = 19.6$ in equation 2.15, corresponds to assuming one value for the VTF parameter, a, ($a = 382$K) in all tissue types. This is still a good approximation since the values of the VTF parameter, a, for the different tissues in figure 3.6b ranges between 371 K and 415 K. This is also obvious in figure 2.1 where data from different biological system were fitted (with an R^2 value of 0.99) in order to derive the new CEM_{43} dose model. If a more precise model is desired, then one can find the VTF parameters (a and A) for a specific type of tissue, and use equation 2.6 as a thermal dose model.

Thermal dose models use relative metrics, the dimensionless Ω in the Arrhenius models,

and t_{43} or t'_{43} [eq.min] in the CEM_{43} models (that theoretically range from zero to infinity) that should be positively correlated to the amount of thermal damage. These dose models are different in the way they quantify thermal damage. Using CEM_{43} models, the dose value can be found independent of the tissue type, and then specific dose threshold for specific tissue types can be used. In Arrhenius models, the Arrhenius parameters are tissue specific and are determined using a reference dose threshold of $\Omega = 1$. Then, the calculated Ω value is mapped to damage extent relative to that threshold. While both metrics were used for producing the results in this work, the thesis concentrates on the CEM_{43} models, since they are simpler and more commonly used.

Chapter 3 presents experimental testing of the new CEM_{43} dose model showing that it is an improvement to the existing model. Figure 3.1 shows the consistency of t'_{43} dose values for the same damage threshold resulting from different time-temperature combinations. Although the data is from the same experiments from which one of the data sets used in deriving the new CEM_{43} dose model was obtained[2,3], the two data sets represent two different damage thresholds. In addition, the same data that was used to derive a dose model can still be used to test its fundamental validity. Using the VTF model (with parameters derived from time-temperature data) to go from dose to time-temperature values as shown in figure 3.7 demonstrates the validity of the VTF model by expecting the time-temperature relation to be close to the original data. This was not the case for the basic Arrhenius model.

More support to the validity of t'_{43} is demonstrated in figure 3.2 which shows survival fraction from thermal exposure against thermal dose values. The survival-dose response was more consistent using the new CEM_{43} dose model compared to the current CEM_{43} model.

Since in thermal therapy treatments temperatures vary spatially and temporally, the new dose model was tested against laser-induced heating experiments which resembles thermal therapy treatments (figure 3.3). The consistency between the current and the new CEM_{43} models in predicting damage thresholds was investigated. Although the method of specifying the thresholds using image processing has some uncertainty, this uncertainty has a

similar effect on both dose models. Using the same damage threshold to defined the boundaries of 6 lesions that were created by different heating protocols tests the consistency of the dose models considering different time-temperature histories. While using two different, arbitrary chosen, thresholds, gives an idea about the sensitivity of that *consistency* to the damage threshold. The results, as shown in section 3.1.3, support the hypothesis that the new CEM_{43} dose model is an enhancement to the current CEM_{43} model.

Since the ultimate goal of thermal dose modelling is to use it in clinical applications, it is important to investigate the clinical relevance of the proven consistency of t'_{43} in predicting damage over a wide range of temperatures. Considering prostate cancer treatment using coagulative thermal therapy, the goal is to cause an irreversible thermal damage to the tumour region which has volume v by delivering thermal dose more than dose threshold (x eq.min) everywhere in tumour region. Meanwhile, a vital organ like the urethra should be spared by receiving thermal dose less than another threshold (y eq.min). Preliminary studies should be done to establish the thresholds x and y parameters in prostate thermal therapy. If these studies where done using the current CEM_{43} dose model with temperatures around 70°C, using these thresholds in a prostate treatment with temperatures around 55°C might cause the urethra to get damaged, because the preliminary studies over-estimated thresholds y by using t_{43} . On the other hand, if the thresholds-establishing studies were done around 55°C, the actual treatment were done around 70°C, and the dose monitoring calculations showed the all volume v had received thermal dose greater than the threshold x, a volume less than v might only get damaged because of the usage of t_{43} . This will leave part of the tumour untreated. The significance of the volume of untreated tumour was investigated using LITT simulations.

Different scenarios, which involve different temporal and spatial distribution of temperatures during treatment, were considered by changing the laser power in the LITT simulations. Different prescribed coagulated volumes and different dose thresholds for the onset of coagulation were investigated as well. In the simulations many tissue parameters change based on

thermal dose values, which leads to a compounding effect by the dose in predicting damage volumes and damage boundaries. The simulations results are shown in figure 3.8.The three figures show that the difference between t_{43} an t'_{43} in predicting damaged volume increases as laser power increases. The second parameter was the dose threshold used to mark the onset of coagulation (threshold x). The deviation between the two models in predicting damaged volume reached 10.8% when the damage threshold was 240 eq.min as shown in figure 3.8a. This value is almost tripled when a threshold of 5,000 eq.min was used as shown in figure 3.8b. This is because higher treatments time are needed to achieve higher threshold at the boundaries for the same prescribed volume. This results in higher temperatures at the boundaries. In both of the previous cases, the prescribed volume of damage was 1 cm^3. In figure 3.8c, the effect of changing the targeted volume was investigated by using 0.5 cm target volume. The deviation in this case reaches 45.9 %. Increasing the power, increasing the threshold, and decreasing the the prescribed volume, all corresponds to higher temperatures at the targeted volume boundaries. This is obvious by looking at the circular markers in figure 3.8 which represent the temperatures at the boundary for each simulations. Since t_{43} increasingly over-estimates damage as temperature increases the deviation increase with any of these changes as the results shows. The significance of the difference supports the importance of using the new CEM_{43} dose model in thermal therapy dose calculations. Using the current model will lead to a damage volume less than the prescribed tumour volume, which will leave part of of the tumour untreated.

Chapter 5

Summary, Conclusion, and Future Work

5.1 Summary and Conclusion

Quantifying thermal damage is very important for clinical applications of thermal therapy. The damage process in biological systems is complicated, and understanding it is not trivial. Thermal damage models assume a first order protein denaturation process in which tissue transforms from native state to denatured state. Protein denaturation is actually more complicated than two states process[23]. Other processes play roles in cell killing due to heat in different range of temperatures, some of them might be unexpected like the phase transformations that happen at threshold values. Neglecting all these complications, thermal dose models are empirical formulae that link exposure time, temperature, and damage extent to each other to form a dose-damage mapping system. Two things are needed to improve thermal dosimetry: more experimental results for a wider range of temperatures in different types of tissue, and new damage models that use experimental result more effectively to produce thermal dose models. This second point is the essence of this work. A new model for CEM_{43} dose calculation has been introduced in this thesis. This dose model

shows more validity and consistency in predicting thermal damage than the existing one. Like the exiting CEM_{43} model, the new model can be used for different types of tissue. The new CEM_{43} model has its explanation in rate process analysis since it was derived based on a modified Arrhenius equation (Vogal–Tammann–Fulcher type). VTF better describes the thermal damage process than the basic Arrhenius equation, as has been shown in this thesis.

The general forms of new dose models were established in this study. Future experiments can result on more accurate values for the constants in equation 2.15 in order to be used in the new CEM_{43} model. *In-vivo*, *ex-vivo*, and controlled cell-culture survival studies can be used for this purpose. While the *in-vivo* experiments resembles the actual treatment the most, the cell-culture experiments have an accurate damage quantifier by counting the survival fraction. The behaviour of the cells in cell-culture experiments might not mimic the behaviour of cells *in-vivo* because it does not include effects like vascular shut-down, or cell-cell signalling. This might be a drawback to cell-culture experiment. If more rigour is needed, one can use the VTF-based Arrhenius-type dose model for a certain type of tissue (equation 2.6) to quantify damage. Since VTF is new to thermal dosimetry studies, new parameters a and A are needed to be derived for different types of tissue. Furthermore, since the relation between the CEM_{43} model and the Arrhenius-type VTF model is established in this work, if the parameter a for a certain type of tissue is determined, it can be used for CEM_{43} calculations.

The hypotheses in this thesis have been validated by showing that the current CEM_{43} model overestimates dose values for higher temperature, and by introducing a more reliable CEM_{43} model based on experimental results. In conclusion, the contribution of this work is introducing methods and mathematical models that will lead to more robust thermal dosimetry. This can lead to improvements in thermal therapy modelling, monitoring, and control.

5.2 Future Work

5.2.1 Thresholds studies

Establishing dose threshold and parameters for different type of tissue, based on the new thermal dose model, is needed. Since the new dose model is more consistent than the current one, these thresholds and parameters will be more useful. The future work can include performing separate studies to find thresholds that represent the minimum dose (in eq.min) needed to cause irreversible damage to tumour tissues that are commonly targeted by heat treatments in tissue such as prostate, liver, and brain. In addition, thresholds that correspond to the maximum dose that tissues of some vital organs can receive without getting damaged, are needed. This will be very important for the clinical usage of thermal therapy.

5.2.2 Optical properties and dose

Dynamic changes in tissue properties due to damage accumulation need to be well described in order to be used in thermal therapy simulation. Dynamic changes in tissue scattering is an example of a property that changes significantly. Molding dynamic changes in tissue scattering is important for simulating treatments that uses optical energy like LITT. The change in scattering due to heat is clear in many examples; like the change of egg white from transparent (low scattering coefficient) to opaque (high scattering coefficient) after heat exposure. As shown in figure 3.3, thermal damage, which is related protein denaturation, is manifested as increases in scattering. Since the change in the scattering coefficient are correlated to thermal damage, it should have a unique relation with thermal dose. This is true , only if, the thermal dose model has an ideal dose–damage mapping system. The data shown in figure 5.1 from Skinner*et al*[4] was used to investigate that.

The data shows the nominalized change in reduced scattering coefficient $\mu_s^{'}$ as function of temperature and time from which thermal dose values can be calculated. The dose was calculated using both t_{43} and $t_{43}^{'}$. Normalized $\mu_s^{'}$-dose responses are shown in figure 5.2

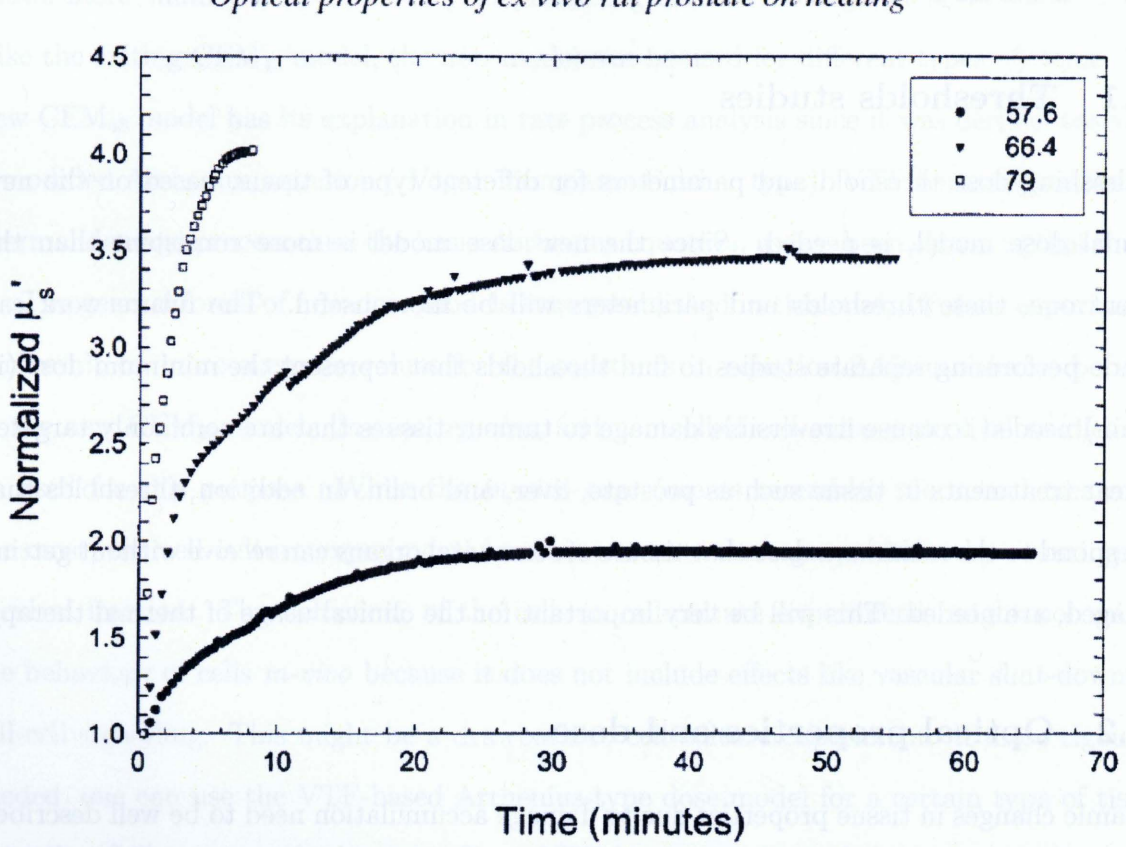

Figure 5.1: Normalized μ_s' as a function of exposure time at three different temperatures for fresh rat prostate from Skinner*et al*[4]. The increase in coagulation leads to an increase in μ_s'.

The change in scattering coefficient is close to a unique relation with t_{43}' , while this is not the case using t_{43} . This again supports the validity of the new CEM_{43} in comparison to the existing one. More importantly, chances in optical properties can, now, be correctly modelled as a function of thermal dose. Future studies are needed find a formula for this relation instead of the one in equation 2.18. Dynamic chances in other tissue properties, that are correlated to thermal damage, can be investigated and molded based on the new CEM_{43} dose model also.

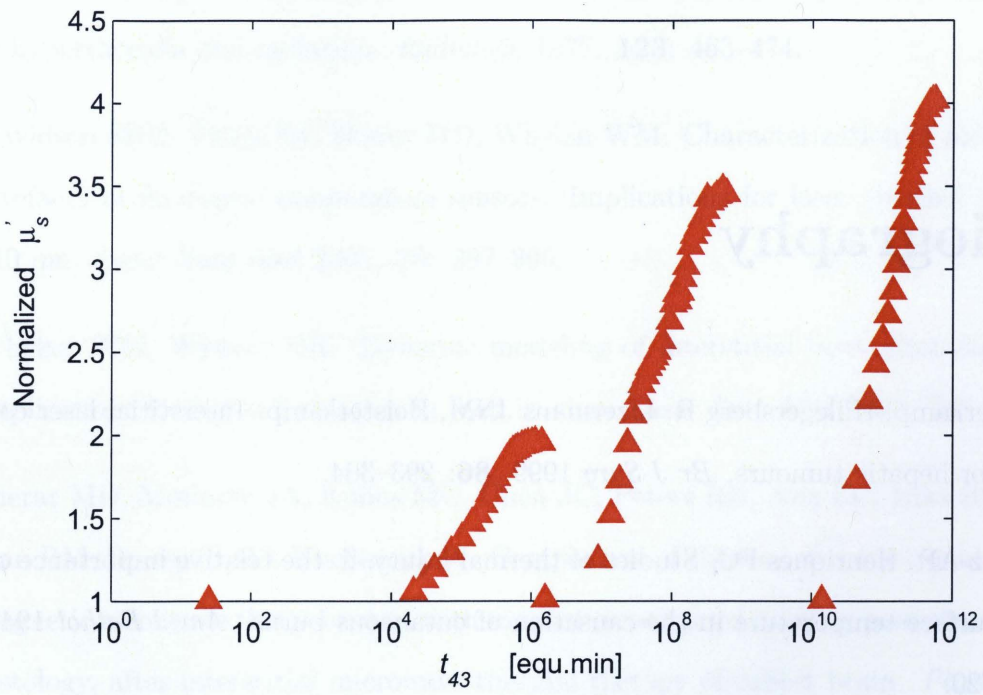

(a)

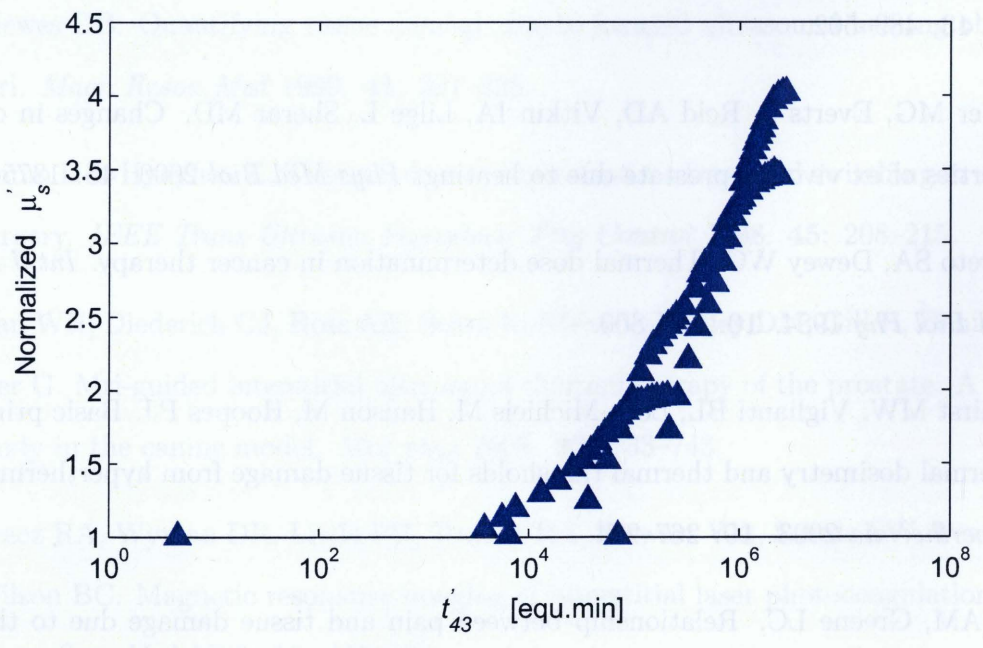

(b)

Figure 5.2: Change in normalized μ_s' as a function of thermal dose. In (a) t_{43} was used in dose calculations, while in (b) t_{43}' was used.

Bibliography

[1] Heisterkamp, Hillegersberg R, IJzermans JNM, Heisterkamp. Interstitial laser coagulation for hepatic tumours. *Br J Surg* 1999. **86**: 293–304.

[2] Moritz AR, Henriques FC. Studies of thermal injury. ii. the relative importance of time and surface temperature in the causation of cutaneous burns. *Am J Pathol* 1947. **23**: 695–720.

[3] Henriques FC. Studies of thermal injury v. the predictability and the significance of thermally induced rate processes leading to irreversible epidermal injury. *Arch Pathol* 1947. **43**: 489–502.

[4] Skinner MG, Everts S, Reid AD, Vitkin IA, Lilge L, Sherar MD. Changes in optical properties of ex vivo rat prostate due to heating. *Phys Med Biol* 2000. **45**: 1375–1386.

[5] Sapareto SA, Dewey WC. Thermal dose determination in cancer therapy. *Int J Radiat Oncol Biol Phy* 1984. **10**: 787–800.

[6] Dewhirst MW, Viglianti BL, Lora-Michiels M, Hanson M, Hoopes PJ. Basic principles of thermal dosimetry and thermal thresholds for tissue damage from hyperthermia. *Int J Hyperthermia* 2003. **19**: 267–294.

[7] Stoll AM, Greene LC. Relationship between pain and tissue damage due to thermal radiation. *J Appl Physiol* 1959. **14**: 373–382.

[8] Dewey WC, Hopwood LE, Sapareto SA, Gerweck LE. Cellular responses to combinations of hyperthermia and radiation. *Radiology* 1977. **123**: 463–474.

[9] Davidson SRH, Vitkin IA, Sherar MD, Whelan WM. Characterization of measurement artefacts in fluoroptic temperature sensors: Implications for laser thermal therapy at 810 nm. *Laser Surg Med* 2005. **36**: 297–306.

[10] Whelan WM, Wyman DR. Dynamic modeling of interstitial laser photocoagulation: Implications for lesion formation in liver in vivo. *Laser Surg Med* 1999. **24**: 202–208.

[11] Sherar MD, Moriarty JA, Kolios MC, Chen JC, Peters RD, Ang LC, Hiks RS, Henkelman RM, Bronskill MJ, Kucharcyk W. Comparison of thermal damage calculated using magnetic resonance thermometry, with magnetic resonance imaging post-treatment and histology, after interstitial microwave thermal therapy of rabbit brain. *Phys Med Biol* 2000.

[12] Graham SJ, Chen L, Leitch M, Peters RD, Bronskill MJ, Foster FS, Henkelman RM, Plewes DB. Quantifying tissue damage due to focused ultrasound heating observed by mri. *Magn Reson Med* 1999. **41**: 321–328.

[13] Daum DR, Hynynen K. Thermal dose optimization via temporal switching in ultrasound surgery. *IEEE Trans Ultrason Ferroelectr Freq Control* 1998. **45**: 208–215.

[14] Nau WH, Diederich CJ, Ross AB, Butts K, Rieke V, Bouley DM, Gill H, Daniel B, Sommer G. Mri-guided interstitial ultrasound thermal therapy of the prostate: A feasibility study in the canine model. *Med phys* 2005. **32**: 733–743.

[15] Tracz RA, Wyman DR, Little PB, Towner RA, Stewart WA, Schatz SW, Pennock PW, Wilson BC. Magnetic resonance imaging of interstitial laser photocoagulation in brain. *Laser Surg Med* 1992. **12**: 165–173.

[16] Chopra R, Tang K, Burtnyk M, Boyes A, Sugar L, Appu S, Klotz L, Bronskill M. Analysis of the spatial and temporal accuracy of heating in the prostate gland using transurethral ultrasound therapy and active mr temperature feedback. *Phys Med Biol* 2009. **54**: 2615–33.

[17] Purdie TG, Lee TY, Iizuka M, Sherar MD. Dynamic contrast enhanced ct measurement of blood flow during interstitial laser photocoagulation: comparison with an arrhenius damage model. *Phys Med Biol* 2000. **45**: 1115–1126.

[18] Gertner MR, Wilson BC, Sherar MD. Ultrasound properties of liver tissue during heating. *Ultrasound Med Biol* 1997. **23**: 1395–1403.

[19] Arora D, Cooley D, Perry T, Skliar M, Roemer RB. Direct thermal dose control of constrained focused ultrasound treatments: Phantom and in vivo evaluation. *Phys Med Biol* 2005. **50**: 1919–1935.

[20] Jain M. A thermal dose controller for laser interstitial thermal therapy. 2007.

[21] Whelan WM, Davidson SRH, Chin LCL, Vitkin IA. A novel strategy for monitoring laser thermal therapy based on changes in optothermal properties of heated tissues. *Int J Thermophys* 2005. **26**: 233–241.

[22] Pearce J, Thomsen S. *Rate process analysis of thermal damage.* Optical-Thermal Response of laser-Irradiated Tissue. New York: Plenum Press, 1995 .

[23] Bischof JC, He X. Thermal stability of proteins. *Ann NY Acad Sci* 2005. **1066**: 12–33.

[24] He X, Wolkers WF, Crowe JH, Swanlund DJ, Bischof JC. In situ thermal denaturation of proteins in dunning at-1 prostate cancer cells: Implication for hyperthermic cell injury. *Ann Biomed Eng* 2004. **32**: 1384–1398.

[25] Chen B, Thomsen SL, Thomas RJ, Oliver J, Welch AJ. Histological and modeling study of skin thermal injury to 2.0 ?m laser irradiation. *Laser Surg Med* 2008. **40**: 358–370.

[26] Henle KJ, Dethlefsen LA. Time-temperature relationships for heat-induced killing of mammalian cells. *Ann NY Acad Sci* 1980. **335**: 234–253.

[27] Civan F. Applicability of the vogel-tammann-fulcher type asymptotic exponential functions for ice, hydrates, and polystyrene latex. *J Colloid Interface Sci* 2005. **285**: 429–432.

[28] Cann DP, Randall CA, Shrout TR. Investigation of the dielectric properties of bismuth pyrochlores. *Solid State Commun* 1996. **100**: 529–534.

[29] Cherif E, Bouanz M. Evidence of vogel-tamman-fulcher bahavior in ionic binary fluids. *Phys Chemistry Liq* 2007. **45**: 649–661.

[30] Kim BM, Jacques SL, Rastegar S, Thomsen S, Motamedi M. Nonlinear finite-element analysis of the role of dynamic changes in blood perfusion and optical properties in laser coagulation of tissue. *IEEE J Sel Top Quantum Electron* 1996. **2**: 922–933.

[31] Welch AJ, Yoon G, Gemert MJCV. Practical models for light distribution in laser-irradiated tissue. *Laser Surg Med* 1987. **6**: 488–493.

[32] Hielscher AH, Alcouffe RE, Barbour RL. Comparison of finite-difference transport and diffusion calculations for photon migration in homogeneous and heterogeneous tissues. *Phys Med Biol* 1998. **43**: 1285–1302.

[33] Nau WH, Roselli RJ, Milam DF. Measurement of thermal effects on the optical properties of prostate tissue at wavelengths of 1,064 and 633 nm. *Laser Surg Med* 1999. **24**: 38–47.

[34] Jaywant SM, Wilson BC, Patterson MS, Lilge LD, Flotte TJMD, etal. Temperature-dependent changes in the optical absorption and scattering spectra of tissues: correlation with ultrastructure. vol. 1882. 1993 pp. 218–229.

[35] Pennes HH. Analysis of tissue and arterial blood temperatures in the resting human forearm. *J Appl Physiol* 1998. **85**: 5–34.

[36] Roggan A, Muller G. *Dosimetry and computer based irradiation planning for laser-induced interstitial thermotherapy (LITT).* Lasers-induced interstitial thermotherapy. Bellingham, Wash.: SPIE Optical Engineering Press, 1995 pp. 488–493.

[37] Lynn B, Cotsell B. The delay in onset of vasodilator flare in human skin at increasing distances from a localized noxious stimulus. *Microvasc Res* 1991. **41**: 197–202.

[38] London RA, Glinsky ME, Zimmerman GB, Bailey DS, Eder DC, Jacques SL. Laser-tissue interaction modeling with latis. *Appl Opt* 1997. **36**: 9068–9074.

[39] Sapareto SA, Hopwood LE, Dewey WC. Effects of hyperthermia on survival and progression of chinese hamster ovary cells. *Cancer R* 1978. **38**: 393–400.

[40] Diaz SH, Nelson JS, Wong BJF. Rate process analysis of thermal damage in cartilage. *Phys Med Biol* 2003. **48**: 19–29.

[41] Arsenault MG, Kolios MC, Whelan WM. Optoacoustic detection of thermal lesions. vol. 7177. 2009 .

[42] Dewey WC. Arrhenius relationships from the molecule and cell to the clinic. *Int J Hyperthermia* 1994. **10**: 457–483.

[43] Wu YC. A modified criterion for predicting thermal injury. *Nat Bur Stand In: Washington, District of Columbia* 1982.